HHS Public Access

Author manuscript

Curr Biol. Author manuscript; available in PMC 2018 July 10.

Published in final edited form as:

Curr Biol. 2017 July 10; 27(13): 1941–1955.e6. doi:10.1016/j.cub.2017.06.004.

Muscle directs diurnal energy homeostasis through a myokine-dependent hormone module in Drosophila

Xiao Zhao[1] and **Jason Karpac**[1,2,*]

[1]Dept. of Molecular and Cellular Medicine, Texas A&M University Health Science Center, College Station, TX 77843, USA

Summary

Inter-tissue communication is critical to control organismal energy homeostasis in response to temporal changes in feeding and activity or external challenges. Muscle is emerging as a key mediator of this homeostatic control through consumption of lipids, carbohydrates, and amino acids, as well as governing systemic signaling networks. However, it remains less clear how energy substrate usage tissues, such as muscle, communicate with energy substrate storage tissues in order to adapt with diurnal changes in energy supply and demand. Using Drosophila, we show here that muscle plays a crucial physiological role in promoting systemic synthesis and accumulation of lipids in fat storage tissues, which subsequently impacts diurnal changes in circulating lipid levels. Our data reveal that the metabolic transcription factor Foxo governs expression of the cytokine Unpaired 2 (Upd2) in skeletal muscle, which acts as a myokine to control glucagon-like adipokinetic hormone (AKH) secretion from specialized neuroendocrine cells. Circulating AKH levels, in turn, regulate lipid homeostasis in fat body/adipose and the intestine. Our data also reveal that this novel myokine-dependent hormone module is critical to maintain diurnal rhythms in circulating lipids. This tissue cross-talk provides a putative mechanism that allows muscle to integrate autonomous energy demand with systemic energy storage and turnover. Together, these findings reveal a diurnal inter-tissue signaling network between muscle and fat-storage tissues that constitutes an ancestral mechanism governing systemic energy homeostasis.

eTOC Blurb

Zhao and Karpac show that Drosophila muscle can systemically control lipid synthesis in fatbody and the intestine. This inter-tissue communication is mediated by a Foxo-dependent myokine (Upd2) and hormonal (AKH) signaling axis, which allows muscle to coordinate diurnal energy demands with fat turnover in tissues that store and synthesize lipids.

[*]Correspondence: karpac@tamhsc.edu.
[2]Lead Contact

Author Contributions

X.Z. performed the experiments, X.Z. and J.K. designed the experiments and wrote the paper.

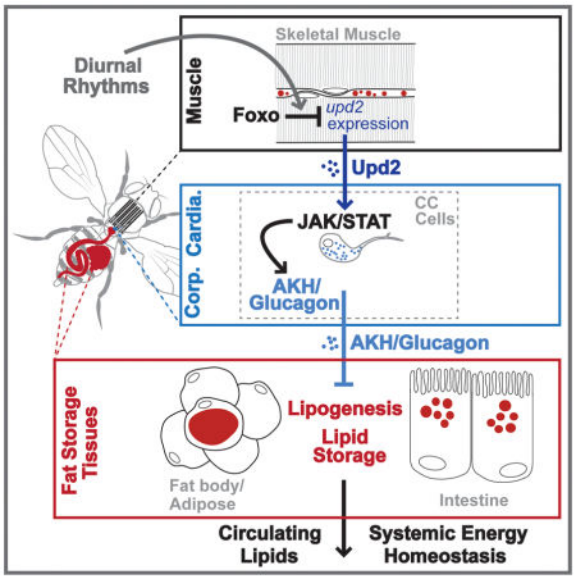

Keywords

muscle; energy homeostasis; diurnal rhythms; tissue cross-talk; lipid metabolism; Foxo; AKH; Upd2; Drosophila

Introduction

Metazoans must maintain energy homeostasis in response to external challenges and internal cues, such as nutrient availability or diurnal rhythms of food intake. This maintenance requires coordinating systemic energy demands between tissues that store and/or use energy substrates, primarily carbohydrates and lipids.

Muscle, specifically skeletal and cardiac, has emerged as a critical mediator of systemic energy homeostasis [1, 2]. As an energy consumer, skeletal muscle directs whole-body energy homeostasis via autonomous energy demand of contracting muscles [3]. The majority of stored energy in many metazoans is in the form of lipids, more specifically triglycerides (TAG). Through the coordination of *de novo* lipid synthesis and lipolysis, the liver and adipose mobilize stored TAG that is consumed by other tissues, including muscle [4–7]. In particular, skeletal muscle shifts to oxidation of lipids (fatty acids), as opposed to glucose, during fasting and physical activity [3, 5]. Lipid absorption, synthesis, and mobilization are also diurnally regulated in order to temporally coordinate energy homeostasis with changes in energy demands during rest-activity and feeding-fasting cycles [8, 9], and muscle lipid consumption is thus under diurnal control [10, 11]. The coordination of energy supply and demand, in response to stress or diurnal rhythms, must therefore require communication between energy storage and usage tissues. Because lipids play an essential role in both normal physiology and pathophysiology, it is critical to understand how energy demands within muscle govern fat metabolism in peripheral tissues that store, synthesize, and mobilize lipids.

Beyond energy substrate consumption, muscle can also secrete humoral factors to regulate systemic energy homeostasis through inter-tissue communication. As an endocrine organ, muscle can shape metabolic changes in distant tissues such as the liver, adipose, and pancreas through the secretion of muscle-derived proteins (myokines), as well as metabolic substrates and intermediates. Various myokines can either independently or cooperatively direct energy homeostasis by regulating multiple aspects of glucose metabolism, lipid metabolism, and insulin sensitivity in other tissues [1, 2, 12–14]). Thus, muscle acts as a key endocrine and metabolic mediator of systemic lipid metabolism that is required to govern energy homeostasis, and understanding how muscle communicates with fat storage tissues to coordinate energy expenditure remains an integral question.

Current work in various model organisms has started to shed light on the transcription factor networks that integrate endocrine and metabolic function in muscle to direct systemic lipid homeostasis. For example, Mediator complex subunit activity, such as MED13, within muscle plays an evolutionarily conserved role in the regulation of lipid accumulation in various tissues [15, 16]. Muscle-specific PGC1-α transcription factor activity can drive changes in the metabolic function of white fat through regulation of the myokine irisin [12]. Additionally, insulin-responsive Forkhead box O (Foxo) transcription factors, conserved signaling integrators required for maintaining metabolic homeostasis, regulate a metabolic switch to lipid usage in skeletal muscle during physical activity, promoting fatty acid uptake and β-oxidation [17–19]. Foxo and PGC1- α, through regulation of the intrinsic circadian clock in metabolic tissues like the liver and muscle, also govern diurnal changes in energy homeostasis [20, 21].

The inter-tissue coordination of systemic lipid metabolism is thus crucial to maintain organismal energy homeostasis and balance the synthesis and breakdown of lipids between organs. Exploiting the unique ability in Drosophila to perform high-throughput, *in vivo* genetic screening in functionally homologous tissues, compared to mammalian counterparts, we uncovered a novel myokine-dependent hormone module that directs systemic lipid metabolism and energy homeostasis. Here, we show that skeletal muscle-specific Foxo activation is required to promote systemic, *de novo* lipid synthesis in fat storage tissues (fat body/adipose and the intestine) in order to maintain hemolymph lipid levels for consumption in other organs. This inter-tissue communication is achieved through the regulation of a myokine-dependent hormone module. Skeletal muscle-specific Foxo activity governs the expression of *upd2*, a putative type I cytokine with functions similar to mammalian leptin [22]. Upd2, in turn, acts as a myokine to control the release of Adipokinetic hormone (AKH; Drosophila glucagon-like signaling) from neuroendocrine cells, highlighting a novel function for Upd2. Circulating AKH levels can subsequently direct lipid homeostasis in fat body/adipose and the intestine. This novel myokine-dependent hormone module is also critical to ensure that diurnal rhythms in circulating lipids, suggesting that muscle-dependent change in systemic lipid homeostasis may be temporally coordinated with feeding and rest-activity cycles. Diurnal regulation of the Upd2/AKH signaling axis provides a mechanism by which muscle can regulate autonomous energy needs by non-autonomously directing lipid synthesis and accumulation in fat storage tissues.

Results

Foxo Function in Muscle Governs Autonomous and Systemic Lipid Homeostasis

Foxo proteins are conserved regulators of energy homeostasis that can promote uptake/usage of lipids in muscle, as well as drive muscle function and dictate systemic physiology [18, 19, 23–25]. Furthermore, fat storage tissues are essential for providing lipids to muscle (Fig. S1A). Due to these catabolic and systemic functions, we hypothesized that Foxo activity in muscle may play a role in balancing autonomous lipid usage with non-autonomous lipid homeostasis in fat storage tissues. To test this, we inhibited the single Foxo ortholog in Drosophila (using UAS-Foxo RNAi [26]) in muscle and assayed organismal lipid storage. Attenuating Foxo function specifically in thoracic skeletal muscle (longitudinal indirect flight muscle; using Act88FGal4, Fig. S1B–C) of female flies results in a 40% decrease in organismal TAG levels at 10 days of age, but no change in TAG content of dissected thoraces (Fig. 1A–B). Similar results were found in male flies (Fig. S1E). Conversely, attenuating Foxo in fat body (similar to mammalian adipose with retained liver-like functions; using CGGal4) or the intestinal enterocytes (using NP1Gal4) leads to either no change or elevated organismal TAG levels (Fig. 1C–D). These data suggest that Foxo function in skeletal muscle uniquely governs organismal lipid homeostasis by non-autonomously modifying fat content in other tissues. To this end, we monitored lipids in skeletal muscle and fat storage tissues (fat body and the intestine) in response to skeletal muscle-specific Foxo attenuation. Using a lipid droplet binding domain-GFP fusion protein (UAS-LD-GFP), we found an autonomous increase of small lipid droplets in longitudinal skeletal muscle sections of Act88FG4>Foxo^{RNAi} flies (Fig. 1E, control co-stains in Fig. S1G–I). Strikingly, the same inhibition of Foxo function in skeletal muscle promotes significant non-autonomous deficits in lipid storage in both the intestine and fat body (Fig. 1F–G), consistent with the overall loss of TAG in these flies (Fig. 1A). Similar results were found utilizing males (Fig. S1D–F) and alternative diets (data not shown), and phenotypes were confirmed with both an independent muscle-specific driver (MHCGal4; Fig. S1J–M) and a second Foxo RNAi transgene (Fig. S2A–G). Overexpressing wild-type Foxo in fly skeletal muscle supported its lipid catabolic role in this tissue, promoting autonomous decreases in lipid storage (Fig. 1H and J), while also elevating total organismal TAG levels (Fig. 1I). Taken together, these data show that Foxo function in skeletal muscle has diverse roles in controlling both autonomous and systemic lipid homeostasis, including a requirement for maintaining lipid accumulation in fat storage tissues.

Muscle Controls Systemic Lipid Synthesis and Circulating Lipid Levels

We next wanted to determine the exact lipid metabolic defect that was limiting fat storage in fat body and the intestine in response to changes in skeletal muscle Foxo activity. Important to note, this dysfunction in lipid homeostasis was not caused by; (i) a disruption in thoracic muscle structure or function (Fig. S3A–B), (ii) a decrease in food intake (these animals appear hyperphagic, Fig. S3C–D), or (iii) a disruption in daily activity rhythms (these animals have normal rhythms but appear hyperactive, Fig. S3E). To gain more insight into these tissue-specific changes in lipid metabolism, we generated genome-wide expression profiles from dissected thoraces (enriched in indirect flight muscle), carcass (enriched in fat body), and intestines of Act88FG4>Foxo^{RNAi} flies. As expected based on the diversity of

tissue function, we observed significant, yet distinct, transcriptome changes in all tissues (Fig. 2A–B and Fig. S4A–D). Gene Ontology (GO) clustering analysis revealed that the most over-represented and significant GO terms from unique tissue transcriptome profiles were related to lipid metabolic processes (for the thorax/muscle and carcass/fat body) and transmembrane transport (for the intestine) associated with down-regulated genes (Fig 2B). A closer look at conserved, transcriptionally regulated genes governing lipolysis, lipogenesis, and beta-oxidation revealed a distinct deviation in lipogenic gene expression between the muscle and fat body/intestine samples (comparing fold change in RPKM values between Act88G4>UAS-Foxo^{RNAi} and Act88FG4>+ controls (Fig. 2C)). These gene sets include regulators of TAG breakdown (such as triglyceride lipases Bmm (mammalian ATGL) and dHSL), *de novo* fatty acid synthesis (such as fatty acid synthase (FASN1) and acetyl CoA carboxylase (ACC)), and fatty acid catabolism (such as Yip2 (mammalian thiolase)), (Fig. 2C). We found that changes in expression of genes controlling lipolysis and beta-oxidation are relatively similar among tissue types in Act88FG4>Foxo^{RNAi} flies. However, changes in expression of genes controlling lipogenesis are decreased in fat body and the intestine in these animals, but are not changed in muscle. Using qRT-PCR, we confirmed the tissue-specific transcriptional divergence in the select genes described above (Fig. 2D–G).

Overall, these genome-wide expression profiles indicate that Foxo activity in skeletal muscle is required to maintain systemic lipid synthesis in certain peripheral tissues. The transcriptomics also revealed a general, cell-autonomous reduction in expression of genes regulating lipid catabolism (beta-oxidation) in muscle (Fig. 2C, G). This may explain why, despite a lack of peripheral fat storage, thoracic skeletal muscle is able to maintain TAG storage/lipid droplets when Foxo function is inhibited (Fig. 1D). The subsequent autonomous increase in small lipid droplets in Act88FG4>Foxo^{RNAi} muscle (Fig. 1D), coupled with the transcriptomic data, also suggests that Foxo plays an important, steady-state role in controlling lipid homeostasis and substrate availability in this tissue.

We next wanted to confirm that these systemic effects on TAG metabolism and storage were due to an underlying defect of lipid synthesis in fat storage tissues. First, we established that organismal decreases in TAG storage in Act88FG4>Foxo^{RNAi} flies was adult-onset and not due to developmental abnormalities (Fig. 3A and Fig. S3F–H). We found that lipid storage defects in tissues first appeared at 5 days of age (after maturation of tissues) and changes in organismal TAG levels emerged at 10 days of age (Fig. 3A and Fig. S3G–H). However, we cannot rule out that these effects are also part of an adaptive response. Next, an assay was used to measure dynamic changes in lipid content based on the incorporation of radiolabeled glucose (^{14}C-glucose) into total lipids during fatty acid synthesis *in vivo*. Both fat body and the intestine are lipogenic [27], but the fly fat body is the primary site for *de novo* lipid synthesis from glucose [28], so we measured glucose-incorporation into total lipids from dissected carcass/fat body. After 30 hrs of eating a diet containing ^{14}C-glucose, carcass/fat body from Act88FG4>Foxo^{RNAi} flies showed a 2 fold decrease in the rate of lipid synthesis (Fig. 3B). We also measured lipid breakdown in these flies (by transferring label-fed flies back to a standard diet (post-fed) without label for 60 hrs), and found no change in the rate of breakdown (Fig. 3C). Finally, transcript levels of *mondo* (mammalian ChREBP, a critical transcriptional regulator of lipogenic gene expression in adult flies [29]) are significantly

reduced in both fat body and the intestine of Act88FG4>Foxo^{RNAi} flies (Fig. 3D). By integrating tissue-specific genome-wide transcriptomics and biochemical analysis, these data highlight a role for skeletal muscle Foxo function in non-autonomously promoting lipogenesis, and thus fat storage, in peripheral tissues. In order to determine how this lipogenic deficit impacted systemic lipid availability, we assessed circulating lipids in the hemolymph of Act88FG4>Foxo^{RNAi} flies. Inhibiting Foxo activity in skeletal muscle leads to significant decreases in circulating lipids (Fig. 3E). This includes attenuation of diacylglycerol (DAG), the major form of transported lipids in Drosophila [30, 31] and TAG in hemolymph, as well as free fatty acids (Fig. 3E). Circulating lipids that are mobilized from the fat body and intestine are a major source of lipid usage/storage in other tissues (Fig. S1A and [31]). Furthermore, decreases in systemic lipid synthesis and circulating lipids leave Act88FG4>Foxo^{RNAi} flies sensitive to metabolic stress (starvation, Fig. 3F). Collectively, these data show that muscle can systemically dictate lipid synthesis and accumulation in peripheral tissues responsible for storing and distributing fats. The systemic coordination of lipid synthesis suggests that muscle can communicate autonomous energy demands with fat body/intestine in order to maintain hemolymph lipid levels for consumption.

AKH Signaling Mediates Muscle-dependent Effects on Systemic Lipid Homeostasis

The systemic coordination of lipid homeostasis is likely to occur through inter-tissue communication between skeletal muscle and fat body/intestine, prompting us to explore potential communication axes. Due to the fact that both fat body and the intestine are concurrently impacted by Foxo attenuation in skeletal muscle, we hypothesized that modulation of a circulating hormone may be responsible for these systemic changes in lipid homeostasis. Chronic Foxo activation in muscle has previously been shown to inhibit food intake, and subsequently attenuate insulin signaling [23]. However, Act88FG4>Foxo^{RNAi} flies are hyperphagic and hyperactive (Fig. S3C–E) and in fact have elevated insulin activity, including increases in AKT phosporylation in the same tissue that displays less fat storage and attenuated lipogenesis (Fig. S3I–J). This may be indicative of other systemic phenotypes driven by Foxo function in muscle (see [23]). Thus, reduced systemic insulin signaling was not a root cause of these tissue-specific lipid homeostasis defects. Adipokinetic hormone (AKH) is another circulating peptide hormone in insects that is the functional ortholog of mammalian glucagon. AKH, similar to glucagon, can regulate organismal carbohydrate and triglyceride metabolism [32, 33]. We therefore determined if Foxo function in skeletal muscle could influence AKH levels. AKH is synthesized and secreted from specialized neuroendocrine cells (putative orthologs of pancreatic α cells [34, 35]) called the corpora cardiaca (CC), which are located anterior to the proventriculus of the gut (Fig. 4A and Fig. S5A). Thus, we imaged hormone localization in these endocrine cells from dissected proventriculus using an AKH-specific antibody. While control flies generally display no or minimal AKH staining, inhibiting Foxo activity in skeletal muscle revealed a significant increase of CC with strong and wide-spread AKH staining among endocrine cells (based on a staining classification system, Fig. 4A–B and Fig. S5A). Quantifying the AKH signal area (relative AKH staining dimensions within the CC, Fig. S5D) also showed that AKH peptides in CC endocrine cells are significantly increased in Act88FG4>Foxo^{RNAi} flies (Fig. 4C). To determine whether this increase in AKH staining correlated with elevated circulating AKH

levels, we measured hemolymph AKH titer by enzyme immunoassay (EIA) using the same antibody and found that Act88FG4>Foxo^{RNAi} flies indeed have increased AKH levels within the hemolymph (Fig. 4D). As a positive control, indicative of elevated AKH signaling, we used wild-type starved animals (Fig. S5B) and as a negative control we used AKH ablated flies (Fig. S5C).

Similar to glucagon, insect AKH has been shown to govern energy homeostasis by driving lipid mobilization from fat storage tissues during starvation [32, 33, 36–38]. However, AKH has also been implicated in controlling lipid synthesis [39], and glucagon has been shown to inhibit lipogenic gene expression (*FAS* and *ACC*) in adipose tissue [40]. We therefore determined if muscle-dependent increases in circulating AKH levels were promoting systemic lipid storage deficits in fat body/adipose and the intestine. Eliminating AKH (using an AKH-specific mutant (*AKH*^{A})) from Act88FG4>Foxo^{RNAi} flies completely rescued the decrease in both organismal TAG levels and circulating lipids in these animals (Fig. 4E–F and added controls in Fig. S5E). Finally, the attenuation of intestinal and fat body lipid storage promoted by muscle-specific Foxo inhibition was rescued in an AKH-mutant background (Fig. 4G–H and Fig. S5F). While Drosophila AKH has primarily been shown to affect lipid homeostasis in fat body through the AKH receptor, AKH can also directly control metabolism in the intestine [41, 42]. Therefore, these AKH-dependent effects on intestinal lipid homeostasis may be direct, or secondary to metabolic changes in the fat body. Taken together, our data suggest that skeletal muscle can direct systemic energy homeostasis through controlling AKH in Drosophila. More specifically, Foxo function in skeletal muscle is required to limit systemic AKH signaling, thus promoting lipid synthesis and accumulation in fat storage tissues, as well as maintaining circulating lipid levels (Fig. 4I).

Muscle-derived Upd2 Governs AKH Levels and Systemic Lipid Homeostasis

The ability of muscle to govern systemic lipid homeostasis through hormonal control allows this tissue to integrate autonomous energy demand with non-autonomous lipid synthesis in fat storage tissues. While our data indicate that Foxo activity in skeletal muscle can control AKH levels in CC endocrine cells, this regulation also represents an additional tissue communication axis that must be resolved (Fig. 4I). We hypothesized that this inter-tissue crosstalk was mediated by a myokine(s). In order to identify potential myokines that could regulate AKH levels in the CC, we explored gene expression changes in putative or previously characterized secreted factors. Analyzing fold change in transcriptome RPKM values of approximately 95 genes that encode secreted factors, we found a striking increase in a particular cytokine, Upd2, when Foxo function was attenuated in skeletal muscle (Fig. 5A, other selected secreted factors highlighted in gray). This increase was confirmed by qRT-PCR (Fig. 5B). Cytokines, in general, are secreted molecules that communicate intercellular signals and play integral roles in controlling invertebrate and vertebrate immune and metabolic homeostasis. Upd2 is one of three related Upd (unpaired) ligands in Drosophila that contain predicted secondary structures similar to that of type I cytokines, and has diverse functions based on spatio-temporal constraints [43, 44]. Other Upds were not increased in Act88FG4>UAS-Foxo^{RNAi} muscle (Fig. S5G). Pertinent to this study, Upd2 has recently been proposed to be the functional homolog of mammalian leptin [22]. In order to determine if Upd2 secreted from skeletal muscle could also play a role in controlling

systemic lipid homeostasis, we first asked whether up-regulation of Upd2 from Foxo-attenuated muscle was driving increases in CC AKH signal. Indeed, inhibiting muscle-derived Upd2 (using RNAi) from Act88FG4>UAS-Foxo^{RNAi} flies completely rescued the observed increases in AKH signal area (Fig. 5C and Fig. S5J–L; and Fig. S5H–I for RNAi efficiency controls).

Upd2, similar to many type I cytokines and leptin, regulates the activity of the conserved JAK/STAT signaling pathway [45]. Upd2 binds the transmembrane cytokine receptor Domeless (Dome), which activates the JAK tyrosine kinase Hopscotch (Hop), which leads to the phosphorylation of the transcription factor STAT92E [43, 44]. In order to determine if changes in AKH levels mediated by muscle-derived Upd2 correlate with JAK/STAT pathway activation in CC endocrine cells, we examined the activity of a STAT reporter (10XSTAT-GFP, previously shown to recapitulate pathway activation [46]). STAT-GFP is present in many CC endocrine cells, and broadly overlaps with AKH signal (Fig. 5D). Furthermore, genetically activating the JAK/STAT pathway specifically in AKH-producing cells within the CC (using an activated form of Hop (AKHGal4>UAS-Hop^{TumL})) resulted in a striking increase in AKH signal (Fig. 5E and Fig. S5J, L). The ability of muscle-derived Upd2, and JAK/STAT pathway activation, to control AKH levels suggested that changes in *upd2* expression would also drive the disruption of lipid homeostasis observed when Foxo function is inhibited in skeletal muscle. Attenuating Upd2 in skeletal muscle significantly rescued the deficit in TAG storage revealed in Act88FG4>UAS-Foxo^{RNAi} flies (Fig. 6A and added controls in Fig. S5M). Muscle-derived Upd2 is also required for promoting the defects in lipid storage in fat body (Fig. 6B–C) and the intestine (Fig. 6D). Furthermore, Upd2 and AKH appear to not impact secondary phenotypes associated with Foxo attenuation in muscle, such as hyperactivity and elevated insulin signaling activity (Fig. S6A–D), indicating a relatively direct Foxo/Upd2/AKH inter-tissue communication axis between muscle and the fat body/intestine.

Thus far, our data support a model by which skeletal muscle can dictate systemic energy homeostasis and lipid synthesis in fat storage tissues through a myokine-dependent hormone module. This inter-tissue communication is first directed by Upd2, acting as a secreted myokine, which is capable of regulating AKH levels within CC endocrine cells and circulating hemolymph. AKH, in turn, represents a circulating hormone that can govern systemic lipid homeostasis (Fig. 6E).

Diurnal Regulation of Muscle-derived Upd2 and AKH Signaling Control Systemic Lipid Homeostasis

We next wanted to explore the normal physiological role for the Upd2/AKH communication axis in the regulation of lipid metabolism. Lipid homeostasis is rhythmically integrated with diurnal feeding and rest-activity cycles, as daily changes in food intake can drive lipid synthesis, absorption, and mobilization [9]. Furthermore, muscle has been shown to shift energy substrate usage, including lipids, in response to diurnal rhythms [7, 8, 47]. Thus, we hypothesized that the Upd2/AKH communication axis may be important for diurnal regulation of energy homeostasis through governing systemic lipid synthesis and circulating lipids levels. To test this hypothesis, we first assessed lipid storage and circulating lipids

during active/feeding phases (LIGHT cycle; Zeitberger Time (ZT) 2–4 (2–4 hrs after light ON) and rest (DARK cycle; ZT14 (2 hrs after lights OFF). It is important to note that all experiments from previous figures were performed during the light cycle at ZT2–4. In control animals, the intestine displayed a strong reduction in lipid storage during the dark cycle (most likely due to decreases in feeding), while the adipose/fat body maintained lipid stores during both phases (Fig. 7A–B). In Act88FG4>UAS-Foxo^{RNAi} flies, the defect in lipid storage in both the intestine and fat body seen during the light cycle persists during the dark cycle (Fig. 7A–B). Total organismal TAG levels also don't change diurnally in controls, but are chronically repressed in both phases when Foxo function is inhibited in muscle (Fig. 7C). However, circulating lipid levels in control animals are diurnally regulated, rising during the light cycle and falling in the dark cycle (Fig. 7D). Act88FG4>UAS-Foxo^{RNAi} flies show a marked reduction in circulating lipids (compared to controls) during the light cycle, but not during the dark cycle (Fig. 7D). Furthermore, food consumption in control animals follows a similar trend as compared to diurnal changes in circulating lipids (higher in the light cycle and lower in the dark cycle, Fig. S3C). The hyperphagia displayed in Act88FG4>UAS-Foxo^{RNAi} flies is only present during the light cycle, when circulating lipids are repressed, and can be affected by re-establishing lipid storage (through attenuating Upd2 or AKH; Fig. S6E–F). Thus, hyperphagia during the light cycle in Act88FG4>UAS-Foxo^{RNAi} flies may be compensatory, responding to low circulating lipid levels.

These data suggest that the Foxo/Upd2/AKH systemic signaling axis may be important for maintaining robust lipid synthesis in fat storage tissues, and promoting circulating lipid levels, in response to diurnal activity/feeding cycles. Chronic repression of this muscle-dependent communication axis thus leads to less fat synthesis and less fat storage. We next wanted to determine if diurnal changes in circulating lipids correlate with diurnal changes in the Foxo/Upd2/AKH axis. Thorax/muscle *upd2* transcription in control animals displayed diurnal rhythms, rising during the dark cycle when circulating lipids are low and the animal is resting (Fig. 7E). Act88FG4>UAS-Foxo^{RNAi} flies show a constant, elevated baseline of thorax/muscle *upd2* transcript levels and thus are absent of rhythmic *upd2* expression (Fig. 7E). AKH signal levels display a similar diurnal rhythm, with AKH signal elevation during the dark cycle (Fig. 7F). Further confirming the diurnal nature of this systemic mechanism, we found that muscle-specific Upd2 is required for the decrease in circulating lipids during rest in the dark cycle, but has no impact during activity/feeding in the light cycle (Fig. 7G). In vertebrates and invertebrates, there is ample evidence that diurnal regulation of lipid metabolism is controlled, in part, by the intrinsic circadian clock system in peripheral tissues [9, 48, 49]. This circadian system includes a core transcription factor/co-repressor network that governs rhythmic gene expression, resulting in metabolic rhythms [9, 50, 51]. To this end, we also found evidence that this network may directly regulate rhythmic *upd2* expression, and that Foxo in turn can control rhythmic expression of certain circadian transcription factors/co-repressors (Fig. S7A–G). These data highlight a putative interaction between Foxo, circadian transcription systems, and cytokine (*upd2)* expression that can govern hormone-dependent metabolic rhythms associated with lipid homeostasis.

Finally, we hypothesized that rhythmic increases in muscle-Upd2 levels and/or JAK/STAT-mediated AKH levels, important for limiting lipid synthesis/circulating lipid levels during rest, may also be critical for inhibiting excessive TAG storage and obesity. Indeed, chronic

(10 days) attenuation of Upd2 in the muscle or JAK/STAT in AKH-producing cells (using AKHGal4 and RNAi against STAT and Hop, as well as a dominant negative form of Dome (ΔCYT)) leads to significant increases in organismal fat storage (Fig. 7H–I).

Discussion

Overall, our results uncover a novel inter-tissue communication axis that governs lipid and energy homeostasis, and highlight how specific tissues can non-autonomously direct metabolism for autonomous energy needs. Muscle in particular has emerged as a central tissue in this systemic coordination of energy homeostasis, and our results identify a muscle-dependent Foxo/Upd2/AKH signaling module that is critical for maintaining lipid homeostasis in peripheral fat storage tissues in the fruit fly. While Drosophila provide an excellent model to genetically dissect signaling circuits important for metabolic control, the highly conserved nature of the ancestral mechanism described in this study suggests that similar signaling systems may be involved in fat storage, energy homeostasis, and even obesity in mammals. We believe that this system can serve as a productive model to address a number of interesting questions relevant to the complex regulation of metabolic and energy homeostasis in metazoans.

Foxo proteins are critical regulators of physiology through tissue-specific roles in regulating energy substrate metabolism [19]. This study highlights the capacity of Foxo to fine tune energy expenditure through autonomous and non-autonomous control of lipid metabolism via muscle. Metabolic transcription factors can thus direct organismal energy homeostasis using customized, tissue-specific systemic signaling mechanisms. The functional output of these systemic signaling mechanisms also appear to be constrained by spatio-temporal or nutritional effects. For example, fat body-derived Upd2 is required to maintain insulin secretion during feeding in Drosophila, and eliminating Upd2 secretion from this tissue leaves flies lean [22]. We show here that muscle-derived Upd2 can elevate systemic AKH signaling, and eliminating Upd2 secretion from muscle results in excessive organismal TAG accumulation. Thus, while there is commonality between myokines and adipokines (adipose-secreted factors), the systemic functions can be variable and programmed. It is important to note that thoracic skeletal muscle is within close physical proximity to the coropora cardiaca endocrine cells that secrete AKH, and therefore muscle-derived Upd2 may be restricted to a paracrine, as opposed to endocrine, signal. Furthermore, the ability of muscle-derived Upd2 to govern lipid homeostasis through AKH signaling, and not insulin, could allow muscle to counterbalance insulin-dependent changes in lipogenesis in order to maintain energy homeostasis. Alternatively, fat body-derived Upd2 may be important for promoting lipid storage through insulin function during the light cycle when food consumption is high, while muscle-derived Upd2 can limit lipid turnover through AKH signaling during the dark cycle.

These tissue-specific and opposing effects on lipid metabolism mediated by a common secreted factor may appear to be a consequence of a limited cytokine pool and a constrained body plan in insects. However, mammals also display commonality between myokines and adipokines that convey diverse roles in regulating systemic glucose and lipid homeostasis [52, 53]. Even the adipokine leptin (of which Upd2 has functional and structural similarities)

can be made and/or secreted from muscle in mice and humans [54, 55]. Our data further imply that muscle-derived leptin might have evolutionarily conserved roles in directing unique aspects of systemic fat metabolism. The unique, tissue-specific function of these secreted factors may also be dictated by the metabolic state of the animal (discussed further below), and thus could be tailored to distinct energy demands and metabolic functions of specific tissues. However, it remains unclear how a common secreted factor, such as Upd2, can elicit selective effects on specific signaling pathways.

Beyond the tissue-specific roles of secreted factors, metabolic functions of hormones can also depend on nutritional context [56]. Both AKH and glucagon can drive the breakdown of stored TAG or the release of fatty acids from adipose [36, 38]. These hormone-dependent effects on lipid metabolism, especially in the case of AKH, require other metabolic changes that are associated with nutrient deprivation (starvation) such as the activation of TAG lipases [38]. Our results suggest that AKH, in the absence of starvation, may also have a significant role regulating systemic lipid synthesis, and subsequently fat storage and circulating lipid levels, in response to diurnal changes in activity and feeding. These results are supported by recent work in Drosophila showing that ectopically increasing AKH levels leads to lean animals without a corresponding increase in metabolic rate [57]. Another recent study provides additional evidence that diet and/or nutrient sensing in the gut can direct AKH signaling activity in the fat body, and subsequently affect circulating carbohydrates [58]. Thus, muscle may able to integrate autonomous energy demands within other inter-tissue communication circuits by governing circulating AKH levels (and influencing AKH signaling) in order to balance carbohydrate and lipid homeostasis.

Exploring how nutritional context can define unique functions of hormones and secreted factors will aid in elucidating systemic mechanisms utilized by specific tissues to integrate autonomous energy demands with non-autonomous energy substrate usage and storage. The Foxo/Upd2/AKH axis can dictate systemic lipid synthesis and circulating lipid levels in the light cycle while food intake is high and substrates, such as carbohydrates, are readily available for *de novo* lipogenesis. This diurnal effect on lipid metabolism could be used to either (i) provide lipids for use in the muscle during active periods in the light cycle, or (ii) to promote lipid uptake (and storage) in the muscle for use during fasting periods in the dark cycle.

Finally, metabolic transcription factors, such as Foxo, appear capable of controlling diurnal energy homeostasis through integration of the circadian clock, metabolism, and energetics [20, 21]. Indeed, a recent study found that phosphorylation of metabolic molecular machinery in the mouse liver is a critical mechanism for circadian control of physiology, which includes rhythmic changes in Foxo phosphorylation [59]. Future work aimed at uncovering the molecular coupling of metabolic transcription factor function and circadian rhythms should clarify the role of muscle in transitioning organismal energy homeostasis during diurnal changes in feeding and activity.

STAR★METHODS

CONTACT FOR REAGENT AND RESOURCE SHARING

Further information and requests for resources and reagents should be directed to and will be fulfilled by the Lead Contact, Jason Karpac (karpac@tamhsc.edu).

EXPERIMENTAL MODEL AND SUBJECT DETAILS

Drosophila husbandry and strains—A detailed list of fly strains used for these studies are provided in the Key Resources Table. All flies were reared on standard yeast and cornmeal based diet at 25°C and 65% humidity on a 12 hr light/dark cycle, unless otherwise indicated. The standard lab diet (cornmeal-based) was made with the following protocol: 14g Agar/165.4g Malt Extract/41.4g Dry yeast/78.2g Cornmeal/4.7ml propionic acid/3g Methyl 4-Hydroxybenzoate/1.5L water.

In order to standardize metabolic results, 2–3 days after eclosion, mated adult flies were placed on a simple sugar-yeast (SY) diet for 10 days. The standard SY diet was made with the following protocol (as previously described in [60]): 1.0g agar/10g sucrose/10g yeast/0.3 ml propionic acid/100 ml water. Ingredients were combined, heated to at least 102°C, and cooled before pouring. All experiments presented in the results were done utilizing female flies except for Fig. S1D–F, Fig. S5I.

The UAS-Foxo^{RNAi} (KK106097) line used throughout the paper was backcrossed 10X into the w^{1118} background used as a control strain. The UAS-DomeΔCYT and UAS-Hop^{TumL} lines were backcrossed multiple generations into the w^{1118} background used as a control strain, and UAS-Stat^{RNAi} and UAS-Hop^{RNAi} were out crossed into this same strain.

METHOD DETAILS

Hemolymph Metabolite Measurements—The thoraces of 40 flies were carefully pierced with a tungsten needle and then placed in a perforated 0.5 ml Eppendorf tube within a 1.5 ml Eppendorf tube. Then, the pierced flies were centrifuged at 4000 rpm for 3 min at 4 °C. The supernatant was carefully collected to avoid debris. Collected hemolymph was centrifuged again at 4000 rpm for 3 min to precipitate debris. The collected hemolymph was used measure metabolites immediately. For TAG/DAG assays, 1 μl of collected hemolymph was diluted with 10 μl of PBST (PBS, 0.1% Tween 20) and used to measure triglycerides/diacylglycerides (StanBio Liquicolor Triglycerides) according to the manufacturer instructions. Samples were normalized to the control group by dividing the glyceride content of each sample by the average of the control samples. Note: The kit measures glycerol cleaved from TAG and DAG, as well as minimal amounts of free glycerol; neutral lipids extracted from hemolymph are comprised of mainly DAG, as well as some TAG [30, 31].

***de novo* Lipid Synthesis Analysis—**After ten days of feeding on standard diet, 200 files were transferred to a standard diet with 2μCi of ^{14}C-labeled glucose. After 30 hr, carcasses of half of the files were dissected in PBS (with all of the eggs and intact intestines removed) and total lipid was extracted from (10 carcasses for each sample; 0 hr sample). The other half were transferred to a fresh standard diet and kept on this food for the next 60

hr (60 hr sample), and then immediately dissected and extracted total lipid from carcass. For extraction of total lipid, 10 carcasses for each sample were homogenized in 2 ml Folch reagent ($CHCl_3$: MeOH 1:1 v/v). Add 0.4 ml cold 0.1 M KCl, vortex 1 min and then spin at 3000 rpm at 4°C for 5 min, then transfer low phase to new glass tube and dry down. The dried lipid was re-suspended in scintillation fluid, and counted (CPM). Zero hour samples indicate the rate of incorporation of glucose into fatty acids and sixty hour samples indicate the breakdown of the labeled fatty acids.

Conditional Expression of UAS-Linked Transgenes—The TARGET system was used in combination with PplGal4 to conditionally express UAS-linked transgenes in fat body (PPLGal4, tub-$Gal80^{ts}$). Flies were developed at 19°C, then shifted to 29°C to induce t ransgene expression post-eclosion (Day 5).

Analysis of Gene Expression—Total RNA from intact fly thorax, heads, carcass and intestines were extracted using Trizol and complementary DNA synthesized using Superscript II (Invitrogen). Real-time PCR was performed using SYBR Green, the Applied Biosystems StepOnePlus Real-Time PCR systems, and the primers pairs described in the extended experimental procedures (Table S1). Results are average ± standard error of at least three independent samples, and quantification of gene expression levels calculated using the ΔCt method and normalized to *actin5C* expression levels.

Western Blot Analysis—Five carcasses were dissected in PBS (All of the eggs and intact intestines were removed), and then homogenized in protein sample buffer; proteins were separated by SDS-PAGE and transferred to nitrocellulose membrane using standard procedures. The following antibodies (all from Cell Signaling) were used: phsopho-Akt (anti-p-Drosophila Akt (S505); rabbit, 1:1000) and beta-actin (anti-beta-actin; rabbit, 1:1000). Signal was detected using HRP-conjugated anti-rabbit and ECL Western Blotting Substrate (Pierce), according to manufacturer instructions. Quantifiaction of signal was measured with Image J; densitometry (normalized to beta-actin).

Metabolite Measurements—For TAG assays, five females (without head) or eight thoraces were homogenized in 200 μl of PBST (PBS, 0.1% Tween 20) and heated at 70°C for 5 min to inactivate endogenous enzymes. Samples were centrifuged at 4000 rpm for 3 min at 4 °C and ten microliters of cleared ex tract was used to measure triglycerides (StanBio Liquicolor Triglycerides Kit) or protein concentrations (Bio-Rad Protein Assay) according to the manufacturer instructions. TAG levels were normalized to weight (for whole animal, measured using MT XS64 scale) or protein level (for thorax), and then normalized to the control group by dividing the triglyceride content of each sample by the average of the control samples. Note: The kit measures glycerol cleaved from TAG and diacylglycerol (DAG), as well as minimal amounts of free glycerol; the majority of neutral lipids extracted from whole flies are TAG [30, 31].

Oil Red O staining—Intact intestines and carcasses (with all of the eggs and intact intestines removed) were dissected in PBS and fixed in 4% paraformaldehyde for 20 min, then washed twice with PBS, incubated for 20 min in fresh Oil Red O solution (6 ml of

0.1% Oil Red O in isopropanol and 4 ml distilled water, and passed through a 0.45 μm syringe), followed by rinsing with distilled water.

Nile Red staining—Carcasses were dissected in PBS (with all of the eggs and intact intestines removed) and fixed in 4% paraformaldehyde for 20 min. Fixed carcasses were then washed twice with PBS, incubated for 30 min in fresh Nile Red solution with DAPI (1μl of 0.004% Nile Red Solution in 500 μl PBS), followed by rinsing with distilled water.

Longitudinal thorax muscle segments were dissected in PBS and fixed with 4% paraformaldehyde for 10 min at room temperature, washed 3 times with PBS for 10 min each, and then incubated with fresh Nile Red solution (2μl of 0.004% Nile Red Solution in 500 μl PBS) for 2 h at room temperature, followed by rinsing with PBS and then staining with DAPI and Alexa Fluor 488 phalloidin (Thermo Fisher Scientific). Identical protocols were used to visualize LD-GFP tagged lipid droplets in muscle.

Confocal images were collected using a Nikon Eclipse Ti confocal system (utilizing a single focal plane) and processed using the Nikon software and Adobe Photoshop.

Immunostaining and Microscopy—For corpora cardiaca AKH staining, intact intestines were fixed at room temperature for 20 min in 4% paraformaldehyde. All subsequent incubations were done in PBS, 0.5% BSA, and 0.1% Triton x-100 at 4°C. The following primary antibodies were incubated overnight at 4°C: rabbit anti-Akh (1:500; Gift of J. Park, University of Tennessee, Knoxville, TN). Alexa Flour-conjugated secondary (Jackson Immunoresearch, 1:500) antibodies were incubated for 2 h at room temperature. Hoechst was used to stain DNA. AKH staining images were collected using a Leica M165FC system (utilizing a single focal plane) and processed using the Leica software and quantified using ImageJ. A blinded experimenter confirmed the original scoring.

For muscle immunostaining, longitudinal thorax muscle segments were dissected in PBS and fixed with 4% paraformaldehyde for 20 min at room temperature, washed 3 times with PBS containing 0.1% Triton X-100 (PBST) and then blocked in blocking buffer (5% BSA in PBST) for 1 h. The primary antibody of Anti-Actinin from Abcam (ab50599, 1:500) was applied overnight at 4°C. Alexa Flour-conjugated secondary (Jackson Immunoresearch, 1:500) antibodies were incubated for 2 h at room temperature. Hoechst was used to stain DNA.

Confocal images were collected using a Nikon Eclipse Ti confocal system (utilizing a single focal plane) and processed using the Nikon software and Adobe Photoshop.

Enzyme immunoassay (EIA) Assay for Quantification of Hemolymph AKH Signal—0.5 μl of hemolymph was diluted with 100 μl PBS and incubated overnight at room temperature in 96-well EIA/RIA plate (corning Incorporated, Corning, NY, USA). Then, hemolymph were cleared from the cells, and bound material in the plate was blocked for 2h with EIA buffer (10 mM Na2HPO4, 3 mM NaH2PO4, 150 mM NaCl, 1 mM NaEDTA·2dH2O, 0.2% Na azide) and 1% BSA. Blocked samples were washed 3 times with PBS-Tween (0.1%) and then treated with 100 μl of anti-Akh antibody at 1:2500 dilution for

1 hour at room temperature. The incubated samples were washed 3 times with PBS-Tween and treated with HRP-conjugated secondary antibody (1:2500) for 1 hour at room temperature. For enzyme reaction, the plate was washed three times with PBS-Tween, then add 100ul of substrate TMB (3, 3′, 5, 5′-teramethylbenzidine; American Qualex antibodies, San Clemente, CA, USA) to each well and incubated 30 min at room temperature. 100ul of 1M phosphoric acid is added to stop the reaction. Samples were quantified by measuring absorbance at 450 nm (A450).

Feeding Behavior—The CAFE assay [61] was done as follows: Briefly, a single fly was transferred from SY standard food to vials filled with 5 ml of 1.5% agar that maintains internal humidity and serves as a water source. Flies were fed with 5% sucrose solution maintained in 5 ul capillaries (VWR, #53432-706). After twelve hours habituation, the old capillaries were replaced with a new one at the start of the assay. The amount of liquid food consumed was recorded after 24 hr and corrected on the basis of the evaporation (typically < 10% of ingested volumes) observed the identical vials without flies. 5 flies were weighed in order to normalize samples.

Feeding assays on blue dye-labeled food were done as follows: 30 flies were transferred from standard food to vials filled with identical medium containing 0.5% brilliant blue. Feeding was interrupted after 1h and 5 flies each were transferred to 50 μl 1 × PBS containing 0.1% Triton X-100 (PBST) and homogenized immediately. Blue dye consumption was quantified by measuring absorbance of the supernatant at 630 nm (A630). Various amounts of dye-containing food were weighed, homogenized in PBST, and measured (A630) in order to create a standard curve used to quantify blue dye food consumption of flies.

Locomotor Activity Rhythms—For locomotor activity experiments, flies were kept for 8 days in 12:12 LD cycles at 25°C. Individual flies were loaded in glass tube s containing standard food and analyzed for locomotor activity using the DAM system (TriKinetics). Activity records were collected in a bin size of 30 min. Locomotor activity data from the last 2 days were averaged, normalized, and calculated.

RNA-Seq Analysis—Intact fly thorax, carcass (with all of the eggs and intact intestines removed) and intestines were dissected in PBS. Total RNA was extracted using Trizol reagent and used as template to generate sample libraries for RNA sequencing (using the TruSeq Stranded Total RNA Library Prep Kit). Sample libraries were sequenced using the Illumina HiSeq 2500. Sequence cluster identification, quality pre-filtering, base calling and uncertainty assessment were done in real time using Illumina's HCS 2.2.58 and RTA 1.18.64 software with default parameter settings. Between 7 and 12 million (1×50) base pair reads were generated per library and mapped to the *Drosophila* genome (Release 6). Expression was recorded as RPKM: reads per kbp per million reads. Gene Ontology clustering analysis was performed using FlyMine [62].

Quantification of ORO and AKH Staining—ORO staining intensity was quantified using Photoshop. Images (anterior midgut for intestines) were collected from light microscopy. These color images were inverted (image > adj. > invert) in Photoshop to obtain

black/white images. Intensity was measured using histogram analysis (mean pixels). Three individual sections (using a constant square area) were measured and averaged within each gut or fat body. Background (inside the gut or around the cuticle (for fat body), but outside of the positive region) was measured and subtracted from each average intensity measurement.

AKH Staining area was quantified using ImageJ. The image scale was set according the image size (Analyze > set scale). The Akh signal was marked using freehand selections tool. The area of marked signal was measured using measure tool (Analyze > measure). At least 10 individual intestines (using a global scale) were measured and averaged.

Climbing assays—Twenty flies were placed into the empty vials, tapped to the bottom, and then given 30 sec. to climb a distance of 6 cm. Flies that successfully climbed 6 cm or beyond in 30 sec were counted. At least 100 total flies (5 cohorts) were used for each genotype tested.

QUANTIFICATION AND STATISTICAL ANALYSIS

All p-values (except those stated below) were calculated using the Student's t test with unpaired samples. The Pearson Chi-square test was used to calculate p-values for starvation sensitivity curves (Fig. 3F and Fig. S1K) and AKH staining (percent in each category, Fig. 4B and Fig. S5K–L) in order to test for significance of frequency distributions. Furthermore, AKH-staining signal area (Figure 4C, Figure 5C, and Figure 7F) was plotted utilizing box plots to highlight distribution of signal area within individual experimental groups.

All error bars represent standard error, and *n* representations are as follows:

Number of whole flies: Figure 1A, C–D, I; Figure 3A, E–F; Figure 4E, Figure 6A; Figure 7C, H–I; FigureS1D, E, J, K; Figure S2B, E; Figure S3B–F; Figure S5E, M; Figure S6C–F; Figure S7E

Number of dissected thoraces/muscle: Figure 1B, J; Figure 2D–G; Figure 5B; Figure 7E; Figure S1A; Figure S5G–H; Figure S7B–D

Number of dissected carcass/fat body: Figure 1G; Figure 2D–G; Figure 3B–D; Figure 4H; Figure 6B; Figure S3H, J; Figure S6A–B; Figure S7F

Number of dissected intestines: Figure 1F; Figure 2D–G; Figure 3D; Figure 4G; Figure 6D; Figure S2G; Figure S3G;

Number of hemolymph samples: Figure 3E; Figure 4D, F; Figure 7D, G; Figure S5B–C;

Number of GFP-labeled lipid droplets: Figure 1E, H

Number of dissected intestines/proventriculus: Figure 4B–C, Figure 5C, E; Figure 7F; Figure S5K–L

Number of dissected abdomens: Figure S1A

Number of dissected heads: Figure S3I

Exact values of all *n*'s can be found in Figure legends.

DATA AND SOFTWARE AVAILABILITY

Data Resources—Raw data files for the RNA sequencing analysis have been deposited in the NCBI Gene Expression Omnibus under accession number GEO: GSE98789.

Supplementary Material

Refer to Web version on PubMed Central for supplementary material.

Acknowledgments

This work was supported in part by the National Institute of Diabetes and Digestive and Kidney Diseases (NIH R01 DK108930 to J.K).

References

1. Baskin KK, Winders BR, Olson EN. Muscle as a "mediator" of systemic metabolism. Cell Metab. 2015; 21:237–248. [PubMed: 25651178]
2. Pedersen BK, Febbraio MA. Muscles, exercise and obesity: skeletal muscle as a secretory organ. Nat Rev Endocrinol. 2012; 8:457–465. [PubMed: 22473333]
3. Kelley DE, Goodpaster B, Wing RR, Simoneau JA. Skeletal muscle fatty acid metabolism in association with insulin resistance, obesity, and weight loss. Am J Physiol. 1999; 277:E1130–1141. [PubMed: 10600804]
4. Chondronikola M, Volpi E, Borsheim E, Porter C, Saraf MK, Annamalai P, Yfanti C, Chao T, Wong D, Shinoda K, et al. Brown Adipose Tissue Activation Is Linked to Distinct Systemic Effects on Lipid Metabolism in Humans. Cell Metab. 2016; 23:1200–1206. [PubMed: 27238638]
5. Horowitz JF. Regulation of lipid mobilization and oxidation during exercise in obesity. Exerc Sport Sci Rev. 2001; 29:42–46. [PubMed: 11210447]
6. Arner P, Bernard S, Salehpour M, Possnert G, Liebl J, Steier P, Buchholz BA, Eriksson M, Arner E, Hauner H, et al. Dynamics of human adipose lipid turnover in health and metabolic disease. Nature. 2011; 478:110–113. [PubMed: 21947005]
7. Liu S, Brown JD, Stanya KJ, Homan E, Leidl M, Inouye K, Bhargava P, Gangl MR, Dai L, Hatano B, et al. A diurnal serum lipid integrates hepatic lipogenesis and peripheral fatty acid use. Nature. 2013; 502:550–554. [PubMed: 24153306]
8. Gnocchi D, Pedrelli M, Hurt-Camejo E, Parini P. Lipids around the Clock: Focus on Circadian Rhythms and Lipid Metabolism. Biology (Basel). 2015; 4:104–132. [PubMed: 25665169]
9. Gooley JJ, Chua EC. Diurnal regulation of lipid metabolism and applications of circadian lipidomics. J Genet Genomics. 2014; 41:231–250. [PubMed: 24894351]
10. Dyar KA, Ciciliot S, Wright LE, Bienso RS, Tagliazucchi GM, Patel VR, Forcato M, Paz MI, Gudiksen A, Solagna F, et al. Muscle insulin sensitivity and glucose metabolism are controlled by the intrinsic muscle clock. Mol Metab. 2014; 3:29–41. [PubMed: 24567902]
11. Hong S, Zhou W, Fang B, Lu W, Loro E, Damle M, Ding G, Jager J, Zhang S, Zhang Y, et al. Dissociation of muscle insulin sensitivity from exercise endurance in mice by HDAC3 depletion. Nat Med. 2016
12. Bostrom P, Wu J, Jedrychowski MP, Korde A, Ye L, Lo JC, Rasbach KA, Bostrom EA, Choi JH, Long JZ, et al. A PGC1-alpha-dependent myokine that drives brown-fat-like development of white fat and thermogenesis. Nature. 2012; 481:463–468. [PubMed: 22237023]
13. Seldin MM, Wong GW. Regulation of tissue crosstalk by skeletal muscle-derived myonectin and other myokines. Adipocyte. 2012; 1:200–202. [PubMed: 23700534]

14. Chung HK, Ryu D, Kim KS, Chang JY, Kim YK, Yi HS, Kang SG, Choi MJ, Lee SE, Jung SB, et al. Growth differentiation factor 15 is a myomitokine governing systemic energy homeostasis. J Cell Biol. 2016
15. Amoasii L, Holland W, Sanchez-Ortiz E, Baskin KK, Pearson M, Burgess SC, Nelson BR, Bassel-Duby R, Olson EN. A MED13-dependent skeletal muscle gene program controls systemic glucose homeostasis and hepatic metabolism. Genes Dev. 2016; 30:434–446. [PubMed: 26883362]
16. Lee JH, Bassel-Duby R, Olson EN. Heart- and muscle-derived signaling system dependent on MED13 and Wingless controls obesity in Drosophila. Proc Natl Acad Sci U S A. 2014; 111:9491–9496. [PubMed: 24979807]
17. Sanchez AM, Candau RB, Bernardi H. FoxO transcription factors: their roles in the maintenance of skeletal muscle homeostasis. Cell Mol Life Sci. 2014; 71:1657–1671. [PubMed: 24232446]
18. Bastie CC, Nahle Z, McLoughlin T, Esser K, Zhang W, Unterman T, Abumrad NA. FoxO1 stimulates fatty acid uptake and oxidation in muscle cells through CD36-dependent and -independent mechanisms. J Biol Chem. 2005; 280:14222–14229. [PubMed: 15691844]
19. Eijkelenboom A, Burgering BM. FOXOs: signalling integrators for homeostasis maintenance. Nat Rev Mol Cell Biol. 2013; 14:83–97. [PubMed: 23325358]
20. Chaves I, van der Horst GT, Schellevis R, Nijman RM, Koerkamp MG, Holstege FC, Smidt MP, Hoekman MF. Insulin-FOXO3 signaling modulates circadian rhythms via regulation of clock transcription. Curr Biol. 2014; 24:1248–1255. [PubMed: 24856209]
21. Liu C, Li S, Liu T, Borjigin J, Lin JD. Transcriptional coactivator PGC-1alpha integrates the mammalian clock and energy metabolism. Nature. 2007; 447:477–481. [PubMed: 17476214]
22. Rajan A, Perrimon N. Drosophila cytokine unpaired 2 regulates physiological homeostasis by remotely controlling insulin secretion. Cell. 2012; 151:123–137. [PubMed: 23021220]
23. Demontis F, Perrimon N. FOXO/4E-BP signaling in Drosophila muscles regulates organism-wide proteostasis during aging. Cell. 2010; 143:813–825. [PubMed: 21111239]
24. IOS, Zhang W, Wasserman DH, Liew CW, Liu J, Paik J, DePinho RA, Stolz DB, Kahn CR, Schwartz MW, et al. FoxO1 integrates direct and indirect effects of insulin on hepatic glucose production and glucose utilization. Nat Commun. 2015; 6:7079. [PubMed: 25963540]
25. Titchenell PM, Chu Q, Monks BR, Birnbaum MJ. Hepatic insulin signalling is dispensable for suppression of glucose output by insulin in vivo. Nat Commun. 2015; 6:7078. [PubMed: 25963408]
26. Karpac J, Biteau B, Jasper H. Misregulation of an adaptive metabolic response contributes to the age-related disruption of lipid homeostasis in Drosophila. Cell Rep. 2013; 4:1250–1261. [PubMed: 24035390]
27. Luis NM, Wang L, Ortega M, Deng H, Katewa SD, Li PW, Karpac J, Jasper H, Kapahi P. Intestinal IRE1 Is Required for Increased Triglyceride Metabolism and Longer Lifespan under Dietary Restriction. Cell Rep. 2016; 17:1207–1216. [PubMed: 27783936]
28. Musselman LP, Fink JL, Ramachandran PV, Patterson BW, Okunade AL, Maier E, Brent MR, Turk J, Baranski TJ. Role of fat body lipogenesis in protection against the effects of caloric overload in Drosophila. J Biol Chem. 2013; 288:8028–8042. [PubMed: 23355467]
29. Mattila J, Havula E, Suominen E, Teesalu M, Surakka I, Hynynen R, Kilpinen H, Vaananen J, Hovatta I, Kakela R, et al. Mondo-Mlx Mediates Organismal Sugar Sensing through the Gli-Similar Transcription Factor Sugarbabe. Cell Rep. 2015; 13:350–364. [PubMed: 26440885]
30. Carvalho M, Sampaio JL, Palm W, Brankatschk M, Eaton S, Shevchenko A. Effects of diet and development on the Drosophila lipidome. Mol Syst Biol. 2012; 8:600. [PubMed: 22864382]
31. Palm W, Sampaio JL, Brankatschk M, Carvalho M, Mahmoud A, Shevchenko A, Eaton S. Lipoproteins in Drosophila melanogaster--assembly, function, and influence on tissue lipid composition. PLoS Genet. 2012; 8:e1002828. [PubMed: 22844248]
32. Galikova M, Diesner M, Klepsatel P, Hehlert P, Xu Y, Bickmeyer I, Predel R, Kuhnlein RP. Energy Homeostasis Control in Drosophila Adipokinetic Hormone Mutants. Genetics. 2015; 201:665–683. [PubMed: 26275422]
33. Lee G, Park JH. Hemolymph sugar homeostasis and starvation-induced hyperactivity affected by genetic manipulations of the adipokinetic hormone-encoding gene in Drosophila melanogaster. Genetics. 2004; 167:311–323. [PubMed: 15166157]

34. Alfa RW, Park S, Skelly KR, Poffenberger G, Jain N, Gu X, Kockel L, Wang J, Liu Y, Powers AC, et al. Suppression of insulin production and secretion by a decretin hormone. Cell Metab. 2015; 21:323–333. [PubMed: 25651184]
35. Kim SK, Rulifson EJ. Conserved mechanisms of glucose sensing and regulation by Drosophila corpora cardiaca cells. Nature. 2004; 431:316–320. [PubMed: 15372035]
36. Jones BJ, Tan T, Bloom SR. Minireview: Glucagon in stress and energy homeostasis. Endocrinology. 2012; 153:1049–1054. [PubMed: 22294753]
37. Bharucha KN, Tarr P, Zipursky SL. A glucagon-like endocrine pathway in Drosophila modulates both lipid and carbohydrate homeostasis. J Exp Biol. 2008; 211:3103–3110. [PubMed: 18805809]
38. Gronke S, Muller G, Hirsch J, Fellert S, Andreou A, Haase T, Jackle H, Kuhnlein RP. Dual lipolytic control of body fat storage and mobilization in Drosophila. PLoS Biol. 2007; 5:e137. [PubMed: 17488184]
39. Iijima K, Zhao L, Shenton C, Iijima-Ando K. Regulation of energy stores and feeding by neuronal and peripheral CREB activity in Drosophila. PLoS One. 2009; 4:e8498. [PubMed: 20041126]
40. Girard J, Perdereau D, Foufelle F, Prip-Buus C, Ferre P. Regulation of lipogenic enzyme gene expression by nutrients and hormones. FASEB J. 1994; 8:36–42. [PubMed: 7905448]
41. Jedlickova V, Jedlicka P, Lee HJ. Characterization and expression analysis of adipokinetic hormone and its receptor in eusocial aphid Pseudoregma bambucicola. Gen Comp Endocrinol. 2015; 223:38–46. [PubMed: 26432101]
42. Bodlakova K, Jedlicka P, Kodrik D. Adipokinetic hormones control amylase activity in the cockroach (Periplaneta americana) gut. Insect Sci. 2016
43. Boulay JL, O'Shea JJ, Paul WE. Molecular phylogeny within type I cytokines and their cognate receptors. Immunity. 2003; 19:159–163. [PubMed: 12932349]
44. Wright VM, Vogt KL, Smythe E, Zeidler MP. Differential activities of the Drosophila JAK/STAT pathway ligands Upd, Upd2 and Upd3. Cell Signal. 2011; 23:920–927. [PubMed: 21262354]
45. Buettner C, Muse ED, Cheng A, Chen L, Scherer T, Pocai A, Su K, Cheng B, Li X, Harvey-White J, et al. Leptin controls adipose tissue lipogenesis via central, STAT3-independent mechanisms. Nat Med. 2008; 14:667–675. [PubMed: 18516053]
46. Bach EA, Ekas LA, Ayala-Camargo A, Flaherty MS, Lee H, Perrimon N, Baeg GH. GFP reporters detect the activation of the Drosophila JAK/STAT pathway in vivo. Gene Expr Patterns. 2007; 7:323–331. [PubMed: 17008134]
47. Xu K, Zheng X, Sehgal A. Regulation of feeding and metabolism by neuronal and peripheral clocks in Drosophila. Cell Metab. 2008; 8:289–300. [PubMed: 18840359]
48. Bass J, Takahashi JS. Circadian integration of metabolism and energetics. Science. 2010; 330:1349–1354. [PubMed: 21127246]
49. Katewa SD, Akagi K, Bose N, Rakshit K, Camarella T, Zheng X, Hall D, Davis S, Nelson CS, Brem RB, et al. Peripheral Circadian Clocks Mediate Dietary Restriction-Dependent Changes in Lifespan and Fat Metabolism in Drosophila. Cell Metab. 2016; 23:143–154. [PubMed: 26626459]
50. Eckel-Mahan K, Sassone-Corsi P. Metabolism and the circadian clock converge. Physiol Rev. 2013; 93:107–135. [PubMed: 23303907]
51. Meireles-Filho AC, Bardet AF, Yanez-Cuna JO, Stampfel G, Stark A. cis-regulatory requirements for tissue-specific programs of the circadian clock. Curr Biol. 2014; 24:1–10. [PubMed: 24332542]
52. Stern JH, Rutkowski JM, Scherer PE. Adiponectin, Leptin, and Fatty Acids in the Maintenance of Metabolic Homeostasis through Adipose Tissue Crosstalk. Cell Metab. 2016; 23:770–784. [PubMed: 27166942]
53. Trayhurn P, Drevon CA, Eckel J. Secreted proteins from adipose tissue and skeletal muscle - adipokines, myokines and adipose/muscle cross-talk. Arch Physiol Biochem. 2011; 117:47–56. [PubMed: 21158485]
54. Wang J, Liu R, Hawkins M, Barzilai N, Rossetti L. A nutrient-sensing pathway regulates leptin gene expression in muscle and fat. Nature. 1998; 393:684–688. [PubMed: 9641678]
55. Wolsk E, Mygind H, Grondahl TS, Pedersen BK, van Hall G. Human skeletal muscle releases leptin in vivo. Cytokine. 2012; 60:667–673. [PubMed: 23010500]

56. Solon-Biet SM, Cogger VC, Pulpitel T, Heblinski M, Wahl D, McMahon AC, Warren A, Durrant-Whyte J, Walters KA, Krycer JR, et al. Defining the Nutritional and Metabolic Context of FGF21 Using the Geometric Framework. Cell Metab. 2016; 24:555–565. [PubMed: 27693377]
57. Gáliková M, Klepsatel P, Xu Y, Kühnlein RP. The obesity - related Adipokinetic hormone controls feeding and expression of neuropeptide regulators of Drosophila metabolism. European Journal of Lipid Science and Technology. 2016
58. Song W, Cheng D, Hong S, Sappe B, Hu Y, Wei N, Zhu C, O'Connor MB, Pissios P, Perrimon N. Midgut-Derived Activin Regulates Glucagon-like Action in the Fat Body and Glycemic Control. Cell Metab. 2017; 25:386–399. [PubMed: 28178568]
59. Robles MS, Humphrey SJ, Mann M. Phosphorylation Is a Central Mechanism for Circadian Control of Metabolism and Physiology. Cell Metab. 2016
60. Skorupa DA, Dervisefendic A, Zwiener J, Pletcher SD. Dietary composition specifies consumption, obesity, and lifespan in Drosophila melanogaster. Aging Cell. 2008; 7:478–490. [PubMed: 18485125]
61. Deshpande SA, Carvalho GB, Amador A, Phillips AM, Hoxha S, Lizotte KJ, Ja WW. Quantifying Drosophila food intake: comparative analysis of current methodology. Nat Methods. 2014; 11:535–540. [PubMed: 24681694]
62. Lyne R, Smith R, Rutherford K, Wakeling M, Varley A, Guillier F, Janssens H, Ji W, McLaren P, North P, et al. FlyMine: an integrated database for Drosophila and Anopheles genomics. Genome Biol. 2007; 8:R129. [PubMed: 17615057]
63. Yu YV, Li Z, Rizzo NP, Einstein J, Welte MA. Targeting the motor regulator Klar to lipid droplets. BMC Cell Biol. 2011; 12:9. [PubMed: 21349165]
64. Hennig KM, Colombani J, Neufeld TP. TOR coordinates bulk and targeted endocytosis in the Drosophila melanogaster fat body to regulate cell growth. J Cell Biol. 2006; 173:963–974. [PubMed: 16785324]
65. Bach EA, Ekas LA, Ayala-Camargo A, Flaherty MS, Lee H, Perrimon N, Baeg GH. GFP reporters detect the activation of the Drosophila JAK/STAT pathway in vivo. Gene Expr Patterns. 2007; 7:323–331. [PubMed: 17008134]
66. Puig O, Marr MT, Ruhf ML, Tjian R. Control of cell number by Drosophila FOXO: downstream and feedback regulation of the insulin receptor pathway. Genes Dev. 2003; 17:2006–2020. [PubMed: 12893776]
67. Cronin SJ, Nehme NT, Limmer S, Liegeois S, Pospisilik JA, Schramek D, Leibbrandt A, Simoes Rde M, Gruber S, Puc U, et al. Genome-wide RNAi screen identifies genes involved in intestinal pathogenic bacterial infection. Science. 2009; 325:340–343. [PubMed: 19520911]
68. Brown S, Hu N, Hombria JC. Identification of the first invertebrate interleukin JAK/STAT receptor, the Drosophila gene domeless. Curr Biol. 2001; 11:1700–1705. [PubMed: 11696329]
69. Sehgal A, Price JL, Man B, Young MW. Loss of circadian behavioral rhythms and per RNA oscillations in the Drosophila mutant timeless. Science. 1994; 263:1603–1606. [PubMed: 8128246]

Highlights

- Muscle Controls Systemic Lipid Synthesis in Fatbody and Intestine
- Foxo-dependent and Muscle-derived Upd2 Governs Systemic AKH Signaling
- Upd2/AKH Direct Inter-Tissue Communication to Control Systemic Lipid Homeostasis
- Diurnal Regulation of Upd2/AKH Dictates Circulating Lipid Levels

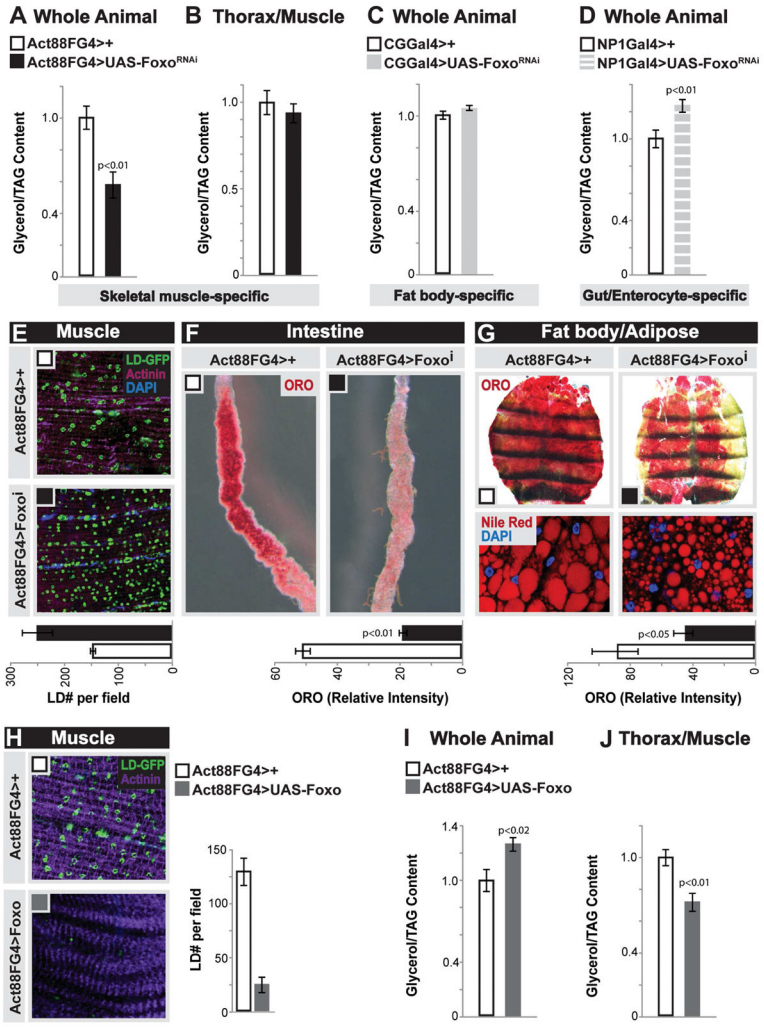

Figure 1. Foxo Function in Muscle Dictates Autonomous and Systemic Lipid Homeostasis

(A–D) Total triglycerides (TAG) levels of whole flies upon Foxo depletion (RNAi line v106097) in fat body (CGGal4), midgut enterocytes (NP1Gal4), or thoracic indirect-flight muscle (Act88FGal4). n=4–8 samples.

(B) TAG levels of dissected thoraces/muscle upon muscle (mu)-specific depletion of Foxo. n=6 samples.

(E–G) Changes in neutral lipid storage upon mu-specific depletion of Foxo

(E) Immunostaining to detect lipid droplets (LD) in dissected longitudinal thoracic muscle; LD (GFP, green), filaments (actinin, purple), and DAPI (blue). Quantification of LD per field, n=8 samples.

(F) Oil red O (ORO) neutral lipid stain of dissected intestines. Intensity quantification of ORO, n=15 samples.

(G) ORO stain and nile red stain (for LD) of dissected carcass/fat body; nile red (red) and DAPI (blue) detected by immunostaining. Intensity quantification of ORO, n=10 samples.

(H) Muscle LD immunostaining and LD quantification (LD; green, GFP and actinin, purple) upon mu-specific induction of Foxo activation. n=5 samples.

(I–J) TAG levels of whole flies and dissected thorax/muscle upon mu-specific induction of Foxo activation. n=5–8 samples.

Bars represent mean±SE. All controls animals represent Act88FGal4>+(w1118).

See also Figure S1, S2, and S3.

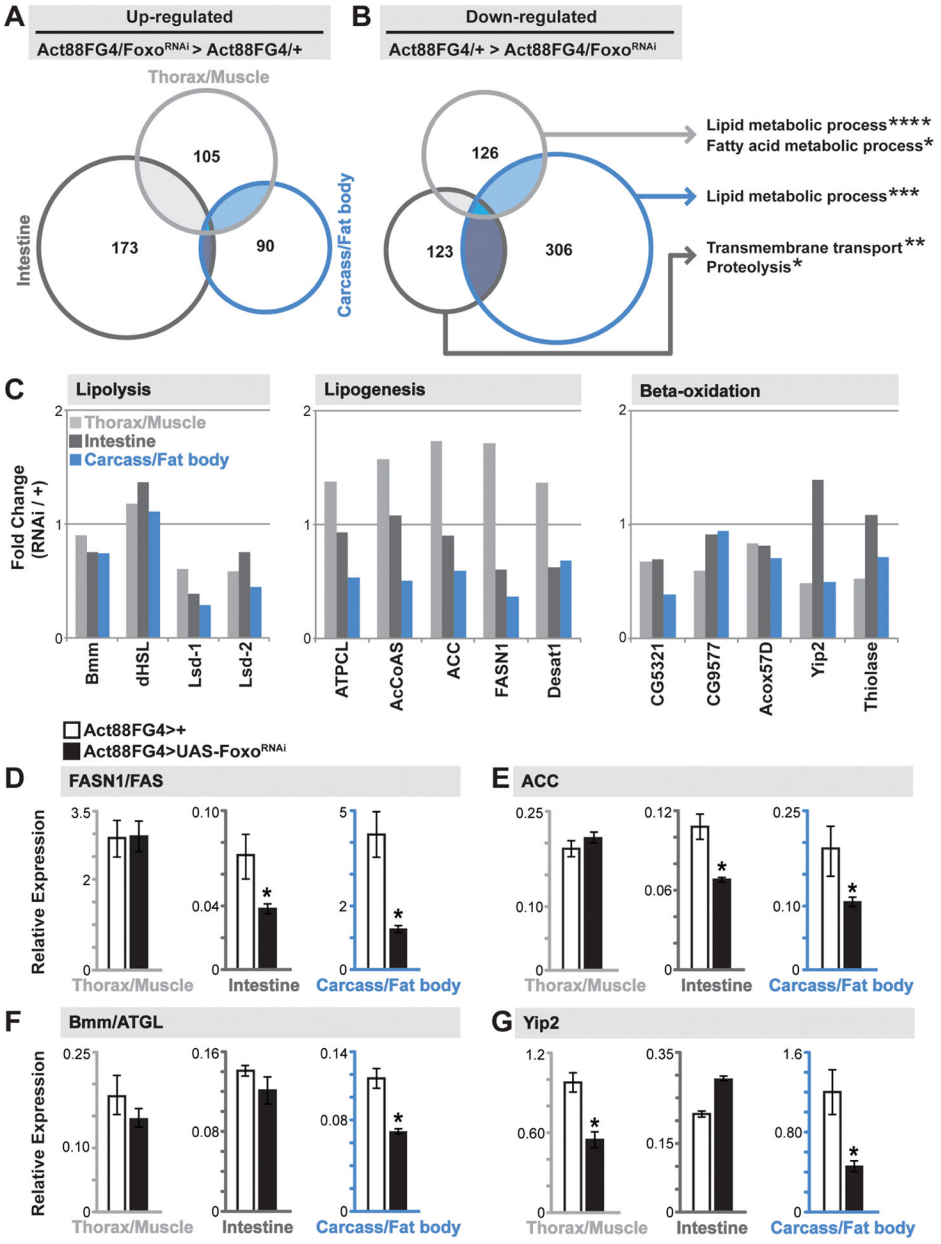

Figure 2. Divergent Tissue-specific Transcriptome Responses to Foxo Depletion in Muscle

(A–B) Venn Diagrams showing autonomously (dissected thorax/muscle) and systemically (dissected carcass/fat body and intestine) up-regulated and down-regulated genes upon mu-specific depletion of Foxo (compared to Act88FGal4>+(w^{1118}) controls). Up- and down-regulated genes were analyzed for Gene Ontology (GO) terms (FlyMine). The threshold for genes included in the analysis was; (i) changes in RPKM values of least 2 fold up- or down-regulated in thorax/muscle and intestine, 2.5 fold in carcass/fat body, compared to controls, and (ii) a minimum RPKM value of 5. Significantly represented GO terms for down-regulated genes for unique tissue transcriptomes (far right). *p-value<0.05; **p-value<0.01; ***p-value<0.001; ****p-value<0.00001.

(C) Fold change (in transcriptome RPKM values, Act88FGal4>FoxoRNAi/Act88FGal4>+ ctrl.) of select genes/enzymes involved in lipolysis (left), lipid synthesis (middle), and lipid oxidation (right) in unique tissues.

(D–G) Drosophila *FASN1*, *ACC*, *bmm*, and *yip2* transcription (measured by qRT-PCR) in unique tissues upon mu-specific depletion of Foxo. Bars represent mean±SE, n=6 samples, *p-value<0.01.

See also Figures S2, S3, S4, and Table S1.

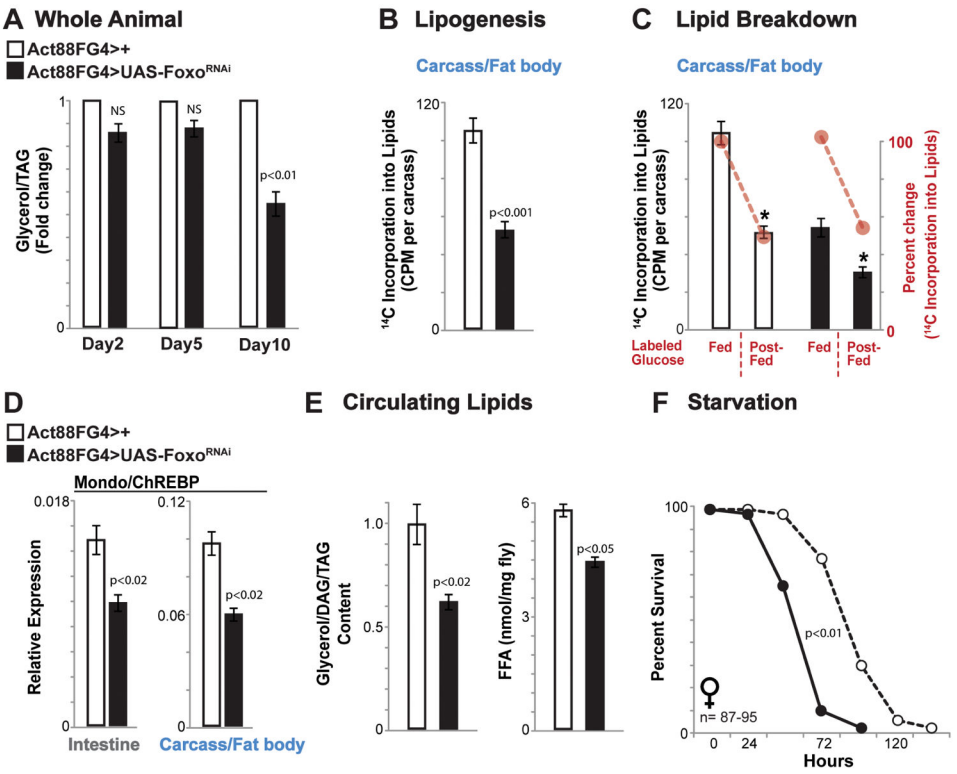

Figure 3. Muscle Controls Systemic Lipid Synthesis and Circulating Lipid Levels

(A–E) Changes in systemic lipid metabolism upon mu-specific depletion of Foxo (A) Fold change in total TAG levels of whole flies during adult maturation (normalized to Act88FGal4>+(w^{1118}) controls). n=4–10 samples, Day 10 time-point re-used from Fig. 1C.

(B) Quantification of *de novo* lipid synthesis via incorporation of diet-fed (30 hrs) ^{14}C-labeled glucose into total lipids from dissected carcass/fat body. n=5 samples.

(C) Quantification of lipid breakdown. Incorporation of ^{14}C-labeled glucose into total lipids (from dissected carcass/fat body) from fed and post-fed (transferred to non-labeled food for 60 hrs) flies. Left axis, total incorporation rates. Right axis (red), percent change (fed/post-fed) for each genotype. Fed data same as panel B. n=5 samples, *p-value<0.01.

(D) Drosophila *mondo* transcription (measured by qRT-PCR) in dissected intestines and carcass/fat body. n=6 samples.

(E) Diacylglycerol (DAG) and TAG levels measured in isolated hemolymph, and free fatty acid (FFA) levels measured in whole flies. n=4–5 samples.

(F) Starvation resistance of female flies.

Bars represent mean±SE. All controls animals represent Act88FGal4>+(w^{1118}).

See also Figure S3 and Table S1.

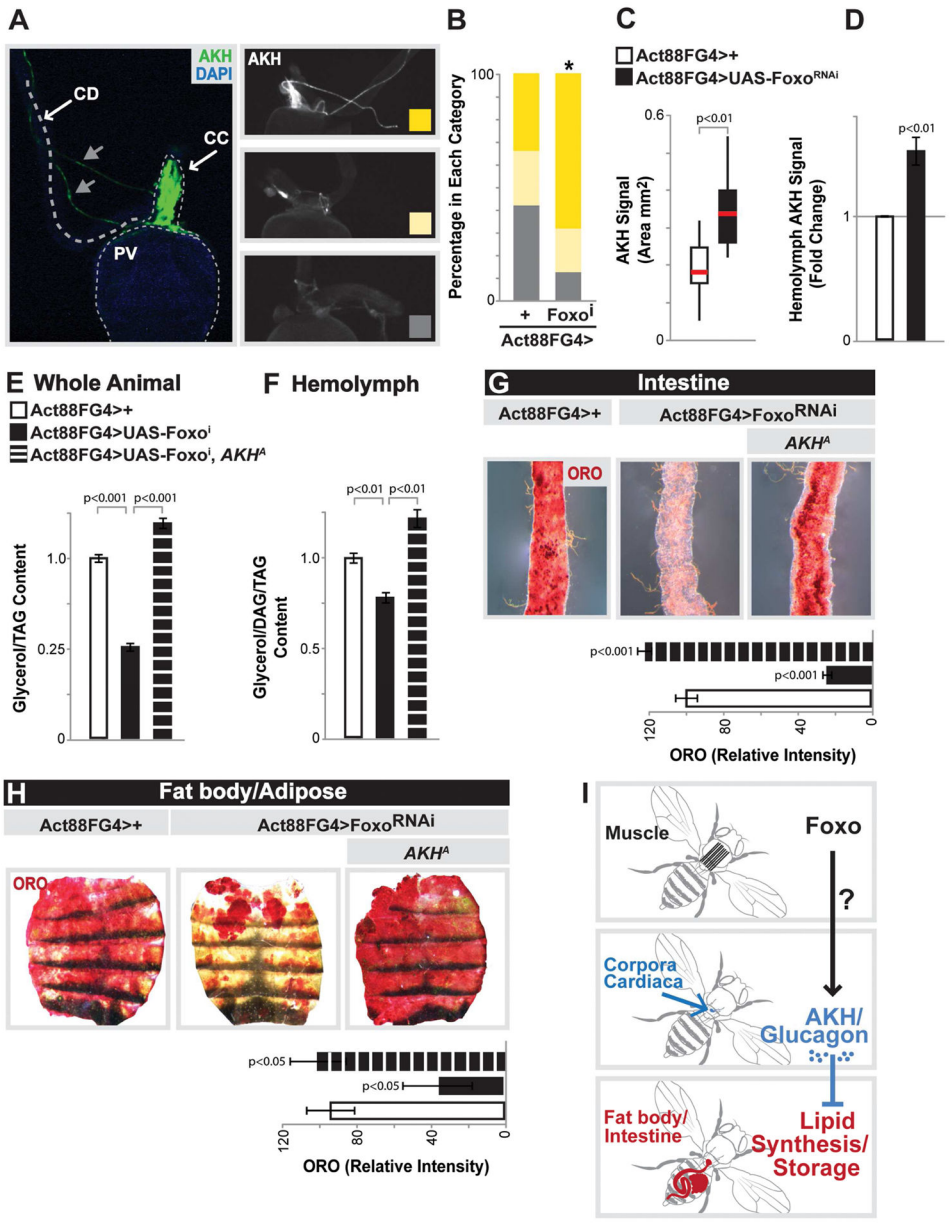

Figure 4. AKH Signaling Mediates Muscle-dependent Effects on Systemic Lipid Homeostasis

(A) AKH immunostaining in the corpora cardiaca (CC). Left panel, anatomical view of AKH producing cells (stained with anti-AKH (green) in the CC, anterior to the proventriculus (PV) of the midgut, with CC axonal projections (gray arrows) and CD (crop duct). PV visualized with DAPI (blue). Right panels, representative images displaying variation in AKH immunostain (white) in CC; high (top), low (middle), and none (bottom).

(B) Quantification of CC AKH immunostain upon mu-specific depletion of Foxo. n=13–18 samples, *p-value<0.01.

(C) Quantification of CC AKH immunostain signal area (mm^2), represented as box plot (median, red line). n=13–15 samples.

(D) Quantification of anti-AKH antibody signal in isolated hemolymph (using enzyme immunoassay (EIA)), fold change compared to Act88FGal4>+ controls. n=5 samples.
(E–H) Total TAG levels of whole flies (n=5 samples), DAG/TAG levels of isolated hemolymph (n=4 samples), and ORO stain of dissected intestines and carcass/fat body upon mu-specific Foxo depletion in the background of an AKH-specific mutant (AKH^{4}). n=5 samples. Intensity quantification of ORO, n=8–15 samples.
(I) Proposed model depicting the communication axis between the muscle, CC/AKH producing cells, and fat storages tissues.
Bars represent mean±SE. All controls animals represent Act88FGal4>+(w^{1118}).
See also Figures S3 and S5.

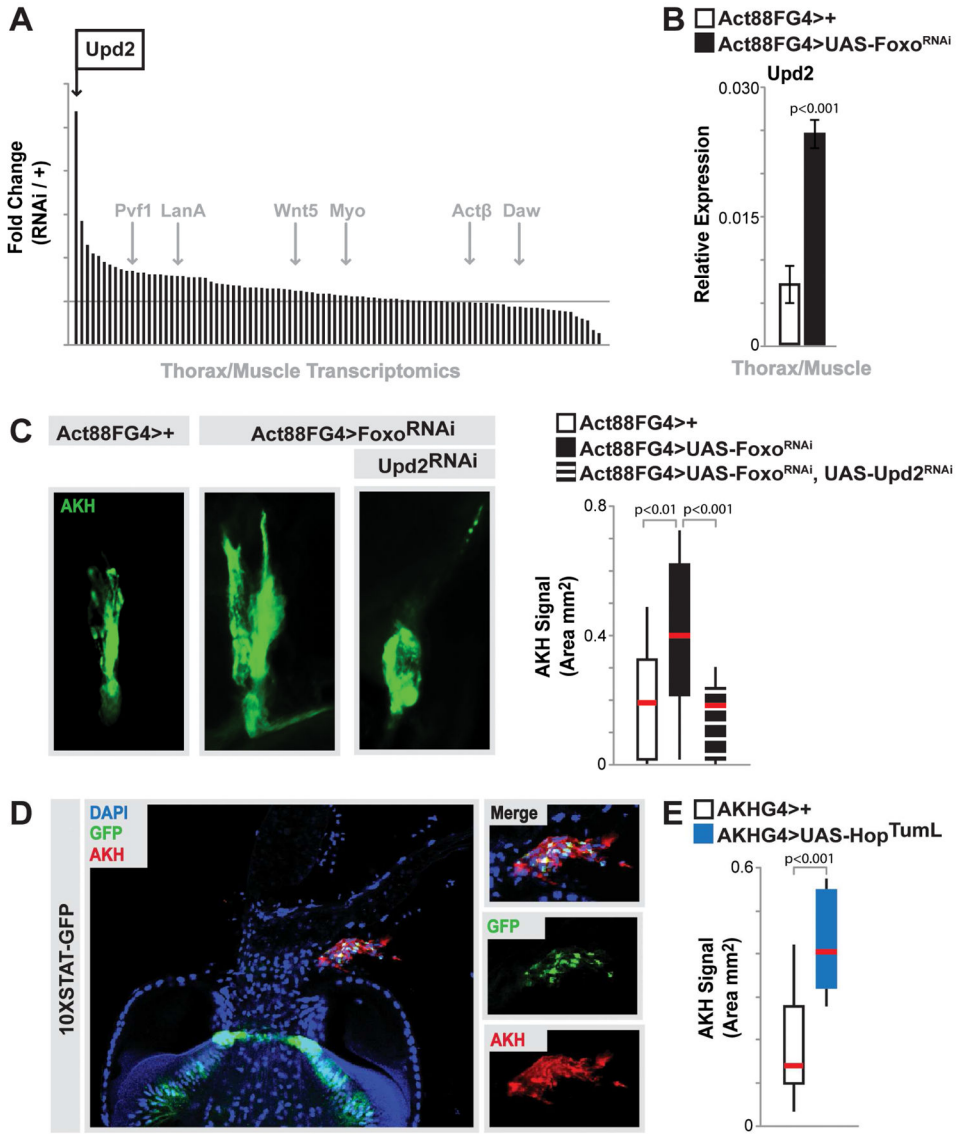

Figure 5. Muscle-derived Upd2 Governs AKH Levels

(A) Histogram plotting fold change (in thorax/muscle transcriptome RPKM values, Act88FGal4>FoxoRNAi/Act88FGal4>+ ctrl.) of genes representing known/putative secreted factors. Upd2 (black arrow) and other known secreted factors (gray arrows) highlighted.

(B) *upd2* transcription (measured by qRT-PCR) in dissected thorax/muscle upon mu-specific depletion of Foxo. n=6 samples. Bars represent mean±SE.

(C) Representative images of CC AKH immunostain (anti-AKH, green) upon mu-specific depletion of Foxo and Upd2 (RNAi line HMS00901). Quantification of immunostain signal area (mm^2), represented as box plot (median, red line). n=12–16 samples.

(D) Proventriculus and CC cells expressing the 10XSTAT-GFP reporter. STAT-GFP (green) expression largely overlaps with AKH immunostain (red) in CC cells, DAPI (blue).

(E) Quantification of CC AKH immunostain signal area (mm^2), represented as box plot (median, red line), upon over activation of Hop (HopTumL) in CC AKH-producing cells (using AKHGal4). n=12–16 samples.

Controls animals represent Act88FGal4>+(w^{1118}) and AKHGal4>+(w^{1118}).
See also Figure S5 and Table S1.

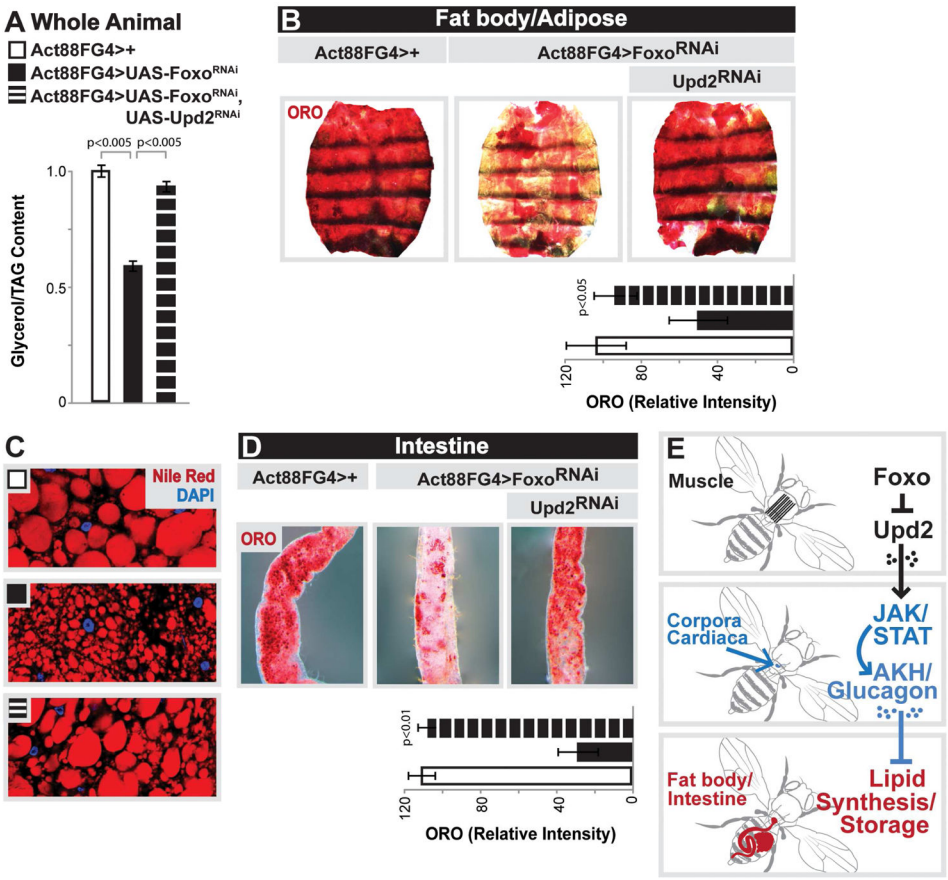

Figure 6. Muscle-derived Upd2 Mediates Muscle-dependent Effects on Systemic Lipid Homeostasis

(A–D) Changes in systemic lipid metabolism upon mu-specific depletion of Foxo and Upd2

(A) Total TAG levels of whole flies. n=5 samples.

(B,D) ORO stain of dissected carcass/fat body and intestines. Intensity quantification of ORO, n=8–15 samples.

(C) Nile red stain (for LD) of dissected carcass/fat body; nile red (red) and DAPI (blue) detected by immunostaining.

(E) Proposed model depicting the communication axes between the muscle, CC/AKH producing cells, and fat storages tissues.

Bars represent mean±SE. All controls animals represent Act88FGal4>+(w^{1118}).

See also Figures S5 and S6.

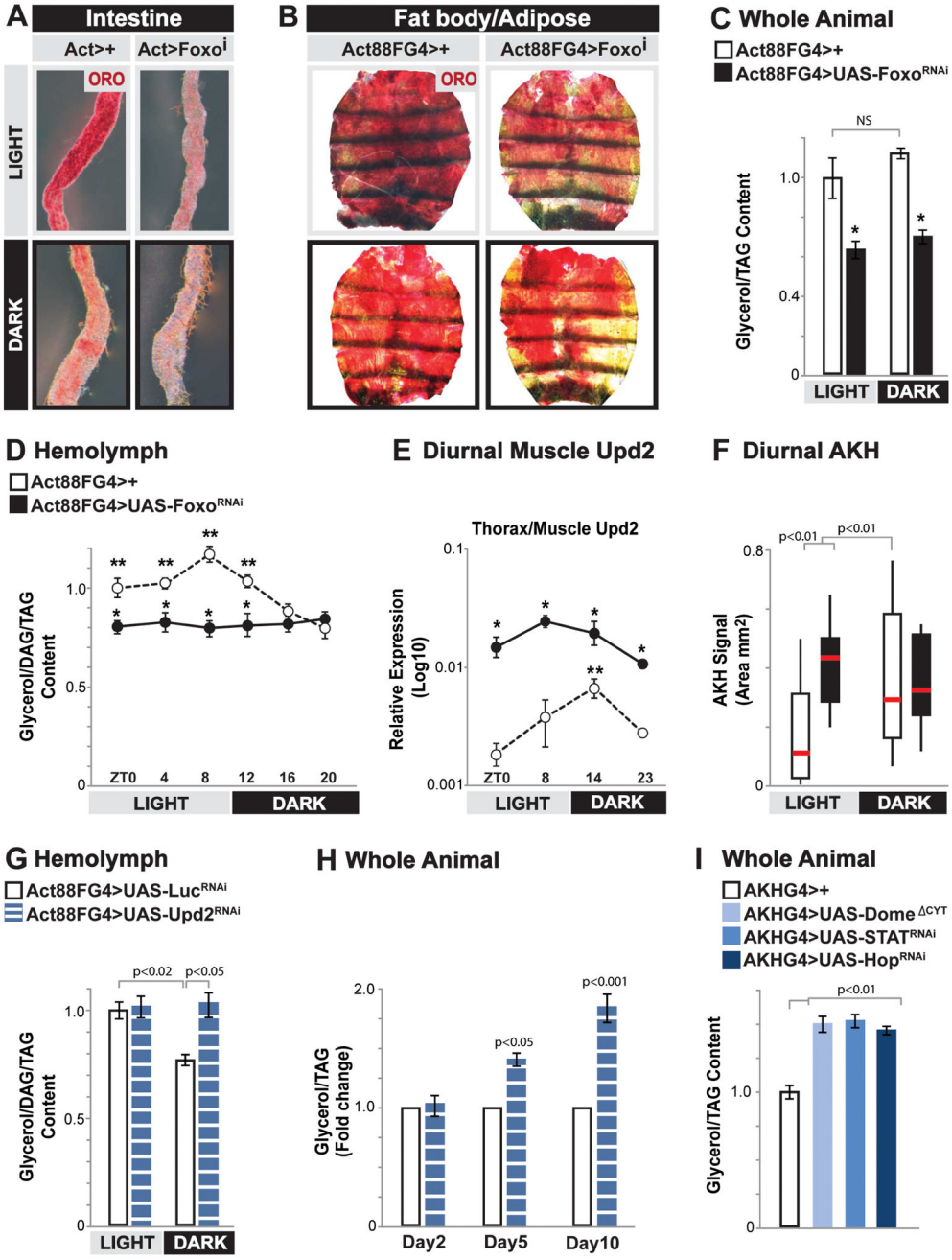

Figure 7. Diurnal Regulation of Muscle-derived Upd2 and AKH Signaling Control Systemic Lipid Homeostasis

(A–B) Representative images from ORO stains of dissected intestines and carcass/fat body during light and dark cycles upon mu-specific depletion of Foxo.

(C) Total TAG levels of whole flies during light and dark cycles upon mu-specific depletion of Foxo. n=3 samples.

(D) DAG and TAG levels measured in isolated hemolymph during light and dark cycles upon mu-specific depletion of Foxo. n=4 samples. *p-value<0.01, designates each ZT data point in the light cycle for Act88FGal4>FoxoRNAi is significant compared to corresponding

ZT data point for controls. **p-value<0.01, designates that each ZT data point in the light cylce of control flies is significant compared to control ZT20 data point.

(E) Diurnal abundance of *upd2* transcription (measured by qRT-PCR) in dissected thorax/muscle from in Act88FGal4>+(w^{1118}) control and Act88FGal4>FoxoRNAi flies. Plotted on Log scale, n=5 samples. *p-value<0.01, designates each ZT data point for Act88FGal4>FoxoRNAi is significant compared to corresponding ZT data point for controls. **p-value<0.001, designates that ZT14 data point of control flies is significant compared to control ZT0 data point.

(F) Diurnal quantification of CC AKH immunostain signal area (mm^2), represented as box plot (median, red line) during light and dark cycles upon mu-specific depletion of Foxo. n=12–16 samples.

(G) DAG and TAG levels measured in isolated hemolymph during light and dark cycles upon mu-specific depletion of Upd2. n=5 samples.

(H) Fold change in total TAG levels of whole flies upon mu-specific depletion of Upd2 during adult maturation (normalized to Act88FGal4>Luc^{RNAi} controls). n=3–6 samples.

(I) Total TAG levels of whole flies upon AKH-producing cell depletion of JAK/STAT signaling (through dominant negative over-expression (DomeΔCYT) and RNAi; STAT and Hop). n=5 samples.

Bars and data points represent mean±SE. Controls animals represent Act88FGal4>+(w^{1118}), AKHGal4>+(w^{1118}), and genetically matched Act88FGal4>LuciferaseRNAi.

See also Figures S3, S6, S7, and Table S1.

KEY RESOURCES TABLE

REAGENT or RESOURCE	SOURCE	IDENTIFIER
Antibodies		
Rabbit polyclonal anti-p-Drosophila Akt	Cell Signaling	4054
Rabbit polyclonal anti-beta-actin	Cell Signaling	4967
Rabbit polyclonal anti-Drosophila Akh	[33]	N/A
Rat monoclonal Anti-Actinin	abcam	ab50599
Goat Anti-Rabbit IgG HRP-conjugate	Biorad	1706515
Alexa Flour 488-conjugated Anti-Rabbit IgG	Jackson Immunoresearch	119191
Cy3-conjugated Anti-Rabbit IgG	Jackson Immunoresearch	119355
Alexa Flour 647-conjugated Anti-Rat IgG	Jackson Immunoresearch	122181
Chemicals, Peptides, and Recombinant Proteins		
^{14}C-labeled Glucose (Glucose, D-[^{14}C(U)])	PerkinElmer	NEC042X050UC
Alexa Fluor 488 Phalloidin	Thermo Fisher Scientific	A12379
DAPI (4′,6-Diamidino-2-Phenylindole, Dihydrochloride)	Thermo Fisher Scientific	D1306
Drosophila Agar, Type II	Genesee	66-103
Malt Extract	Genesee	62-110
Inactive Dry yeast	Genesee	62-106
Cornmeal	Genesee	62-101
Propionic acid	VWR	TCP0500-500mL
Methyl 4-Hydroxybenzoate	VWR	97061-946
Sucrose	VWR	97063-788
Folch reagent	This paper	N/A
Trizol	Life Technologies	15596018
Superscript II Reverse Transcriptase	Life Technologies	18064022
iTaq Universal SYBR Green Supermix	Biorad	1725121
Nitrocellulose membrane	VWR	10600006
Oil Red O	abcam	ab150678
Nile Red	Life Technologies	N1142
Phosphoric acid	VWR	97064-780
Brilliant blue	Sigma-Aldrich	B0149
ECL Western Blotting Substrate	Pierce	32106
Critical Commercial Assays		
StanBio Liquicolor Triglycerides Kit	Fisher	SB-2100-430
Bio-Rad Protein Assay	Bio-Rad	5000006
EIA buffer	This paper	N/A
TMB Soluble Substrate	VWR	EMCL07-100
TruSeq Stranded Total RNA Library Prep Kit	Illumina	RS-122-2203
Deposited Data		

REAGENT or RESOURCE	SOURCE	IDENTIFIER
Raw and analyzed RNA sequencing data	This paper	GEO: GSE98789
Experimental Models: Organisms/Strains		
D. melanogaster: w^{1118}	Bloomington Drosophila Stock Center	BDSC: 3605; FlyBase: FBst0003605
D. melanogaster: w*; P{ppl-GAL4.P}2	Bloomington Drosophila Stock Center	BDSC: 58768; FlyBase: FBst0058768
D. melanogaster: P{tubP-GAL80ts}20	Bloomington Drosophila Stock Center	BDSC: 65406; FlyBase: FBst0065406
D. melanogaster: UAS-Foxo RNAi (y^1sc*v^1; P{TRiP.HMS00793}attP2)	Bloomington Drosophila Stock Center	BDSC:32993; FlyBase: FBst0032993
D. melanogaster: UAS-upd2 RNAi (y^1sc*v^1; P{TRiP.HMS00901}attP2)	Bloomington Drosophila Stock Center	BDSC:33949; FlyBase: FBst0033949
D. melanogaster: UAS-Apoltp RNAi (y^1sc*v^1; P{TRiP.HMC03294}attP2)	Bloomington Drosophila Stock Center	BDSC:51937; FlyBase: FBst0051937
D. melanogaster: UAS-Rfabg/Apolpp RNAi (y^1v^1; P{TRiP.HM05157}attP2)	Bloomington Drosophila Stock Center	BDSC:28946; FlyBase: FBst0028946
D. melanogaster: UAS-Rfabg/Apolpp RNAi (y^1sc* v^1; P{TRiP.HMS00265}attP2/TM3)	Bloomington Drosophila Stock Center	BDSC:33388; FlyBase:FBst0033388
D. melanogaster: y1 w*; P{UAS-Akh.L}2	Bloomington Drosophila Stock Center	BDSC:27343; FlyBase: FBst0027343
D. melanogaster: y1 v1 hop^{Tum}/FM7c	Bloomington Drosophila Stock Center	BDSC:8492; FlyBase: FBst0008492
D. melanogaster: UAS- luciferase RNAi (y^1v^1; P{TRiP.JF01355}attP2)	Bloomington Drosophila Stock Center	BDSC: 31603; FlyBase: FBst0031603
D. melanogaster: w*; P{Act88F-GAL4.1.3}3	Bloomington Drosophila Stock Center	BDSC: 38461; FlyBase: FBst0038461
D. melanogaster: w*; P{Mhc-GAL4.K}2/TM3, Sb1	Bloomington Drosophila Stock Center	BDSC: 55133; FlyBase: FBst0055133
D. melanogaster: w*; P{w[+mC]=GAL4-ninaE.GMR}12	Bloomington Drosophila Stock Center	BDSC: 1104; FlyBase: FBst0001104
D. melanogaster: UAS-Foxo RNAi (y^1w*; P{KK108485}VIE-260B)	Vienna Drosophila RNAi Center	VDRC: 106097; FlyBase: FBst0477923
D. melanogaster: UAS-Hop RNAi (w*; P{GD9157}v40037/CyO)	Vienna Drosophila RNAi Center	VDRC: 40037; FlyBase: FBst0463355
D. melanogaster: UAS-Stat RNAi (y^1w*; P{KK100519}VIE-260B)	Vienna Drosophila RNAi Center	VDRC: 106980; FlyBase: FBst0478803
D. melanogaster: w*; P{UASp-LD-GFP}	[63]	N/A
D. melanogaster: w*; P{CG-GAL4.A}	[64]	N/A
D. melanogaster: w*; P{10x-Stat92E-GFP}	[65]	N/A
D. melanogaster: w*; AKH^A	[32]	N/A
D. melanogaster: w*; P{UAS-Foxo}	[66]	N/A
D. melanogaster: w*; NP1-GAL4 (P{GawB}Myo31DF^{NP0001})	[67]	N/A
D. melanogaster: w*; P{UAS-$Dome^{\Delta CYT}$}	[68]	N/A
D. melanogaster: w*; tim^{01}	[69]	N/A
D. melanogaster: w*; per^{01}	[69]	N/A
Oligonucleotides		

REAGENT or RESOURCE	SOURCE	IDENTIFIER
Primers for ACC, see Table S1	This paper	N/A
Primers for FASN1, see Table S1	This paper	N/A
Primers for Yip2, see Table S1	This paper	N/A
Primers for Bmm, see Table S1	This paper	N/A
Primers for Mondo, see Table S1	This paper	N/A
Primers for Thor, see Table S1	This paper	N/A
Primers for Dilp2, see Table S1	This paper	N/A
Primers for Dilp3, see Table S1	This paper	N/A
Primers for Dilp5, see Table S1	This paper	N/A
Primers for Upd2, see Table S1	This paper	N/A
Primers for Upd1, see Table S1	This paper	N/A
Primers for Upd3, see Table S1	This paper	N/A
Primers for CLOCK, see Table S1	This paper	N/A
Primers for Per, see Table S1	This paper	N/A
Primers for Tim, see Table S1	This paper	N/A
Software and Algorithms		
ImageJ	NIH Image	https://imagej.net/ImageJ
FlyMine	[62]	http://www.flymine.org/flymine/begin.do
Illumina's HCS 2.2.58 and RTA 1.18.64	Illumina	N/A
Other		
DAM (Drosophila Activity Monitor) system	TriKinetics	N/A
Illumina HiSeq 2500	Illumina	N/A
StepOnePlus Real-Time PCR systems	Applied Biosystems	N/A
Leica M165FC system	Leica	N/A
Nikon Eclipse Ti confocal system	Nikon	N/A
Capillaries	VWR	53432-706
96-well EIA/RIA plate	VWR	29442-322